JBC RESEARCH ARTICLE

KDM5A methylation modulates its genomic demethylase and transcriptional actions

Received for publication, August 4, 2025, and in revised form, March 19, 2026 Published, Papers in Press, April 8, 2026
https://doi.org/10.1016/j.jbc.2026.111436

Tram Anh Tran[1], Gokul Gopinathan[1], Clarissa G. Nuñez[1], Frank Goodavish[1], Shwu-Yuan Wu[2,3], Randy Tran[1], Andrew Lemoff[3], Luc Girard[1,4], and Elisabeth D. Martinez[1,2,4,*]

From the [1]Hamon Center for Therapeutic Oncology Research, UT Southwestern, Medical Center, Dallas, Texas, USA; [2]Simmons Comprehensive Cancer Center, Medical Center, Dallas, Texas, USA; [3]Department of Biochemistry, UT Southwestern, Medical Center, Dallas, Texas, USA; and [4]Department of Pharmacology, UT Southwestern, Medical Center, Dallas, Texas, USA

Reviewed by members of the JBC Editorial Board. Edited by Brian D. Strahl

Members of the KDM5 family of Jumonji histone demethylases have been implicated in a variety of human diseases, including multiple cancers and neurological disorders. The regulation of KDM5 enzyme levels and activity, however, are poorly understood. Here we report that KDM5A is methylated by SMYD2 and that this methylation decreases histone demethylase activity and partly alters the KDM5A protein interactome. A mutant KDM5A that can no longer be modified at K1063 exhibits unique genomic sites of action, demethylates H3K4me3 more robustly across the genome and at new loci, has stronger and unique transcriptional effects, and distinct protein-protein interactions. As a result, a number of cell proliferation pathways are affected, and cancer cell growth is blunted. This study illustrates the functional consequences of post-translational modifications of lysine residues in KDM enzymes impacting genomic histone demethylation, gene expression, protein-protein interactions and growth signaling, and establishes lysine methylation as a regulatory event in KDM5A action.

Members of the Jumonji family of lysine demethylases, or JmjC KDMs, were discovered 20 years ago and have been the subject of widespread research due to their impact on the genome's transcription and on other DNA-related processes. These enzymes are involved in human disease, including many solid and blood malignancies, metabolic and neurological disorders and cardiomyopathies (1–14), among others. At the biochemical level, the activity of JmjC KDMs is dependent on Fe^{2+}, molecular oxygen and α-ketoglutarate to carry out the hydroxylation and full demethylation of histone and other protein substrates (15–17). Little else is known, however, about the regulation of JmjC KDM catalytic activity. Post-translational modifications of KDMs themselves represent a potential layer of control over their enzymatic activity and cellular functions. Indeed, functionally impactful post-translational modifications have been recently described for a few KDMs (18–21).

Among JmjC KDMs, the H3K4me3/2 demethylase KDM5A has established roles as a transcriptional repressor due to its ability to erase this generally activating histone mark, and functions in DNA repair and transcriptional plasticity (22). KDM5A has been described as oncogenic in many settings, and it has wide-reaching impact beyond cancer, in autism disorders, inflammation, autophagy, and metabolism among other processes (20, 22–24). Directly or indirectly, this enzyme has also been found to regulate aspects of cell division by its interaction with nucleosome and kinetochore components and to affect RNA processing and translation (22, 25–28). Whether the same or distinct forms of KDM5A are involved in all these processes remains an open question. No post-translational modifications with functional consequences have been reported for KDM5A.

Here we uncover a regulatory mechanism modulating KDM5A activity through lysine methylation. We present evidence demonstrating that the lysine methyltransferase SMYD2, which has multiple non-histone substrates (29–35), methylates KDM5A at K1063. This methylation event leads to a significant decrease in the H3K4me3 demethylase activity of KDM5A. Conversely, we show that mutation of this lysine abrogates methylation and increases KDM5A demethylase activity in cells, leading to expanded changes in gene expression. Furthermore, we explore the functional consequences of this methylation-dependent regulation of KDM5A in the context of cellular proliferation and KDM5A's protein interactions. Our findings reveal that the KDM5A lysine mutant, exhibiting heightened demethylase activity, leads to a decrease in cell proliferation rates, likely through the observed changes in cell cycle and energy production gene expression. In addition, an important interaction with the COMPASS component WDR5 is lost upon methylation of KDM5A, among others. Together, this suggests that the SMYD2-mediated methylation of KDM5A acts as a molecular switch to fine-tune its enzymatic activity, its genomic and protein-protein associations and its effects on cellular growth. These findings provide new insights into the intricate regulatory network governing KDM5A function and its action on cellular physiology and disease processes.

* For correspondence: Elisabeth D. Martinez, elisabeth.martinez@utsouthwestern.edu.

© 2026 THE AUTHORS. Published by Elsevier Inc on behalf of American Society for Biochemistry and Molecular Biology. This is an open access article under the CC BY-NC-ND license (http://creativecommons.org/licenses/by-nc-nd/4.0/).

Results

SMYD2 methylates KDM5A at K1063

We originally set out to evaluate if KDM5A had demethylase activity on non-histone proteins including p53 which is methylated by SMYD2. Although we did not observe this demethylation, we noticed that KDM5A had incorporated SAM in the presence of SMYD2. We therefore focused on defining post-translational modifications that may regulate KDM5A stability or function given its oncogenic properties in human tumors and its role in neurological disorders and autism (23, 36–43). Mass spectrometry analysis of recombinant KDM5A 1 to 1090 revealed various methylation sites (Table S1). Methylation has not yet been studied on KDM5 enzymes but has been reported for at least two other Jumonji family members (18, 19). To validate the methylation of KDM5A we performed *in vitro* methylation assays with purified candidate methyltransferases SMYD2 and with G9A as a control methyltransferase (Fig 1*A*, left panel). SMYD2 and G9A represent two major modes of methylation catalysis. Methylation assays revealed that SMYD2 but not G9A methylated KDM5A robustly, although G9A was highly active on a histone substrate and thus catalytically intact (Fig. 1*A*). Furthermore, a catalytically dead SMYD2 (Y240F) lacked the ability to methylate KDM5A (39), as expected (Fig. 1*B*, right panel). Quantification of the radioactive methyl group transferred onto KDM5A by SMYD2 from the labeled SAM methyl donor revealed that about 30% of KDM5A was methylated assuming monomethylation only events, consistent with mass spectrometry data (Fig. 1*B*, left panel). This % methylation is similar to the methylation levels of the known SMYD2 substrate p53 (29) in the same assay (Fig. 1*C*). To evaluate if SMYD2 methylates endogenous KDM5A, we overexpressed SMYD2 in HEK-293T cells and immunoprecipitated endogenous KDM5A. We then analyzed this KDM5A immunoprecipitate by Western blot using a pan-anti mono/di methyl lysine antibody to detect methylation. This showed strong methylation of KDM5A in the SMYD2 overexpressing cells compared to the empty vector control cells (Fig. 1*D*), indicating that at least under high SMYD2 conditions, KDM5A is methylated in cells.

We then analyzed by mass spectrometry recombinant KDM5A methylated *in vitro* by SMYD2 to identify potential methylation sites. Two lysines within human KDM5A were methylated primarily (K222) or exclusively (K1063) after incubation with SMYD2 per mass spectrometry analysis (Table S1, column "SMYD2-dependent?"). To identify which of these was acted on by SMYD2, we synthesized peptides containing 20 amino acids around these two sites, with either the WT lysines or the corresponding alanine mutations. We then used these peptides in methylation reactions *in vitro* and this showed that SMYD2 robustly methylated K1063 but not K222 (Fig. 1*E*). This is consistent with K1063 being part of an LK consensus sequence found in SMYD2 substrates (44) which is lacking at K222 (Fig. S1*A*). Indeed, LK at 1062/1063 is found specifically in KDM5A but not in KDM5B (Fig. S1*A*). It is also found in KDM5C and KDM5D although these KDMs lack a PHD3 domain found in KDM5A and KDM5B. Analysis of mutations in human cancer of this LK site in KDM5A did not find clear evidence of lysine mutations, yet we did find evidence of the leucine being mutated to phenylalanine (Fig. S1, *A–B*), a mutation that is thought to have functional consequences per COSMIC prediction (45). Structural modeling demonstrated that K1063, although not near the catalytic site, may affect KDM5A function through interactions with the nearby PHD2 domain (Fig. S1*B*).

Having identified a site of methylation *in vitro*, we next generated a point mutation in full-length KDM5A and assessed whether wild-type (WT) *versus* K1063A mutant (MUT) KDM5A was methylated by SMYD2 in cells. We transfected either WT or MUT HA-tagged KDM5A at similar levels (or an empty vector control, EV) into HEK-293T cells along with catalytically active (CA) or catalytically inactive (CI) SMYD2, or an EV control. The ectopically expressed HA-tagged KDM5A was immunoprecipitated using an anti-HA antibody. HA-tagged KDM5A was detected by the anti-HA antibody in all the samples that were transfected with HA-tagged KDM5A (WT or MUT) but was not detected in cells that were transfected with EV, showing the selectivity of the pull-down (Fig. 1*F*, INPUT). Lysine methylation was then assessed in these HA-immunoprecipitants by Western blot using a pan-anti mono/di methyl lysine antibody. Methylated KDM5A was only detected in cells co-expressing full-length WT HA-tagged KDM5A and CA SMYD2 but not in cells expressing WT HA-KDM5A with CI SMYD2 nor in cells expressing MUT HA-KDM5A with CA or CI SMYD2 (Fig. 1*F*, IP), although SMYD2 expression was robust (Fig. 1*F*, INPUT) and HA-KDM5A pull downs similarly efficient (Fig. 1*F*, IP). These results establish that full-length KDM5A is methylated in cells by SMYD2, that this requires SMYD2's catalytic activity and that methylation requires K1063.

KDM5A methylated at K1063 has lower histone demethylase activity and acquires new protein interactors

To determine if methylation of KDM5A at K1063 had functional consequences and could be regulatory, we performed mock (heat inactivated SMYD2) or full (active SMYD2) methylation reactions on recombinant KDM5A 1 to 1090 and then subsequently used this KDM5A in histone demethylase activity assays with exogenous H3K4me3 as the substrate for demethylation (Fig. S2*A*). ELISA assays measuring the demethylated H3K4me2 histone product reported that while the KDM5A that was not *in vitro* methylated retained full demethylase activity, the SMYD2-methylated KDM5A enzyme was catalytically defective and showed significantly reduced demethylating capacity compared to its unmethylated counterpart (Fig. 2*A*). These results were confirmed by independent Western-analysis read outs, which again showed that the mock-methylated KDM5A control (H.I. SMYD2 lane) generated more H3K4me2 product (right panel) and retained less of the original H3K4me3 substrate (left panel) than the methylated KDM5A (SMYD2 lane) (Fig. 2*B*). Thus, by two independent measurements the methylated

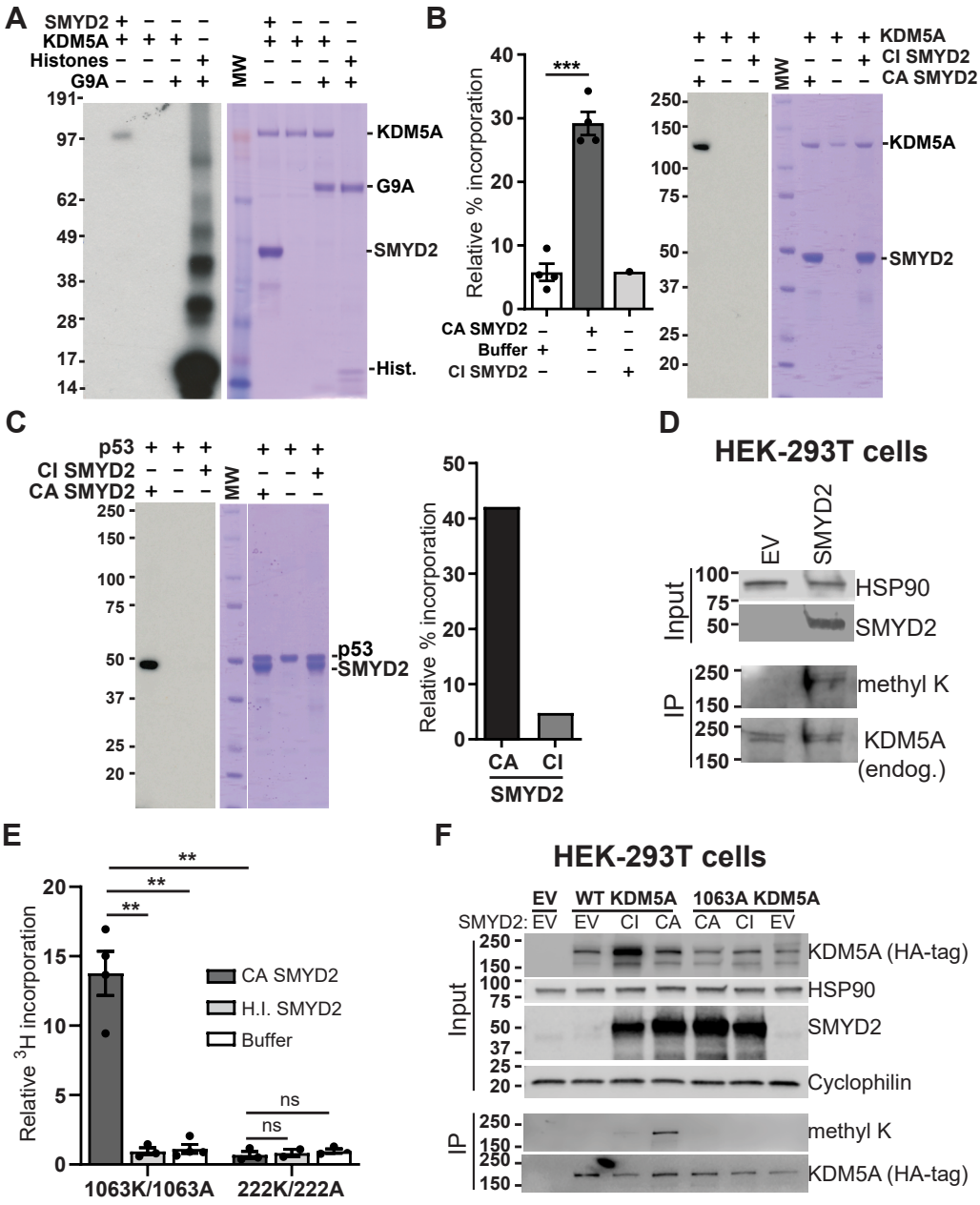

Figure 1. SMYD2 but not G9A methylates KDM5A. *A*, radiograph (*left*) and Coomassie gel (*right*) of methylation of KDM5A by SMYD2 but not G9A. However, G9A could methylate its known substrate, histones. *B*, catalytic activity of SMYD2 is required for KDM5A methylation. *Left*, quantification of ^{3}H methyl group incorporated into KDM5A. Average values were graphed with error bars representing SEM, buffer n = 4, Wt SMYD2 n = 4, catalytic inactive Y240F SMYD2 (CI) n = 1. Percent shown assumes mono-methylation only, although di or tri maybe possible; only monomethyl was detected by mass spectrometry in parallel samples. *Right*, radiograph and Coomassie gel of methylation of KDM5A by wild type SMYD2, but not catalytic inactive Y240F SMYD2. The purified KDM5A in (*A*) and (*B*) came from the same source with the expected molecular weight of 125 kDa as measured by two different MW ladders. In (*A*), KDM5A ran between 97 and 191 kDa markers while in (*B*), it ran between 100 and 150 kDa markers. *C*, left, radiograph and Coomassie gel (*right*) of SMYD2-mediated methylation of p53. *Right*, quantification of ^{3}H methyl group incorporated into p53, n = 1. MW, molecular weight. *p*-values are from *t* test, 2-tailed, paired. *D*, Western blot analysis of HEK-293T cells overexpressing SMYD2 (Input) and probed for endogenous KDM5A methylation. KDM5A was immunoprecipitated then probed with a pan-methyl (mono/di) lysine antibody. KDM5A levels pulled down were equivalent in EV *versus* SMYD2 transfected cells. A signal for pan-methyl lysine was only observed in KDM5A IP from the SMYD2 overexpressed cells (IP). The original red signal of SMYD2 (detected by Cmyc antibody) was converted to grayscale and displayed as pseudocolor. *E*, KDM5A is methylated at residue 1063 by SMYD2. Twenty amino acid peptides around residues 222 or 1063 (wild type, K, or alanine mutant, *A*) were used for methylation assays using SMYD2 as enzyme and ^{3}H-SAM as methyl group donor. Incorporation of the ^{3}H methyl group into wild type peptides was normalized to the ^{3}H incorporation into corresponding alanine mutants. Data are average and SEM, n = 3. *p*-values are from *t* test, 2-tailed, unequal variance. *, $p \leq 0.05$, **, $p \leq 0.01$, ***$p \leq 0.001$. *F*, Western blot analysis for methylation levels of immunoprecipitated full length HA-tagged WT or MUT KDM5A in cells expressing catalytically active (CA) or catalytically inactive (CI) exogenous SMYD2 or EV controls. HA-tagged KDM5A (WT or MUT) expressed in HEK-293T in the presence of overexpressed SMYD2 (CA or CI) (input) was immunoprecipitated (IP) using an anti-HA antibody. IP products were probed with a pan-methyl (mono/di) lysine antibody or with KDM5A with an anti-HA antibody. The original red signals of SMYD2, HSP90, and cyclophilin were converted to grayscale and are displayed as pseudocolored.

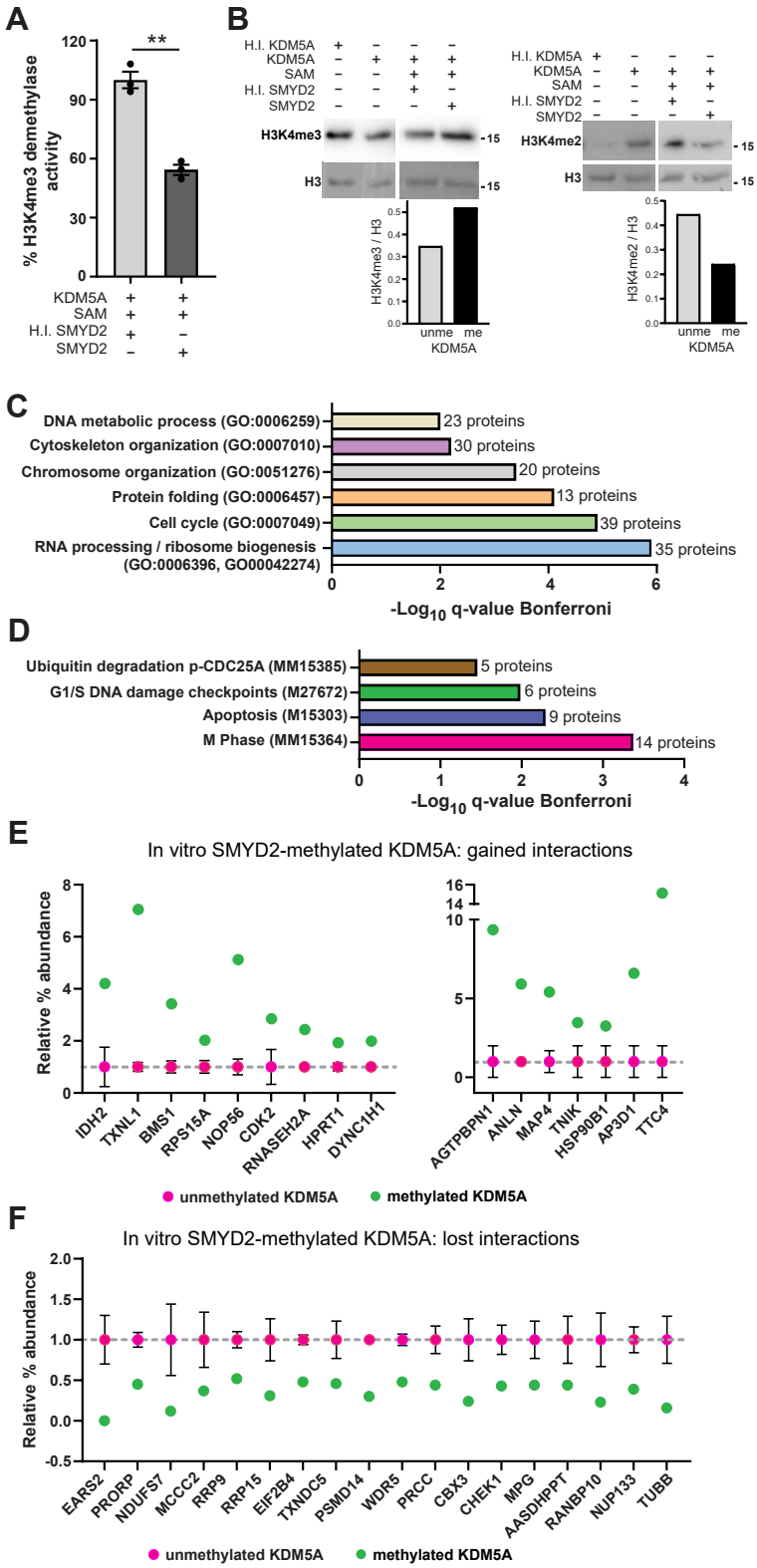

Figure 2. SMYD2-Methylated KDM5A shows reduced activity and acquires new protein interactors *in vitro*. *A*, ELISA-based demethylase assay of KDM5A after its methylation by SMYD2 using H3K4me3 peptide as the substrate. H.I., heat inactivated. **, $p \leq 0.01$, *p*-values are from *t* test, 1-tailed, unequal variance, n = 3. *B*, Western blot-based demethylase activity assay using histone H3K4me3 as substrate. The *left panel* shows control basal levels of H3K4me3 (H.I. KDM5A) and demethylated levels after incubation with active enzyme (KDM5A), followed by H3K4me3 levels after incubation with active KDM5A or KDM5A methylated *in vitro* by SMYD2. The *right panel* depicts the corresponding H3K4me2 levels before and after KDM5A incubation showing increased H3K4me2 in reactions that decreased H3K4me3. Quantification is show under the western blots. *C*, significant GO terms corresponding to methylated KDM5A unique/preferred binding proteins revealed by TOPPGENE analysis. *D*, significant GO terms corresponding to unmethylated KDM5A unique/preferred binding proteins. *E* and *F*, relative percent total abundance of HEK-293T cell lysate proteins that bind to mock methylated (HI SMYD2 or

KDM5A had lower demethylase activity on H3K4me3 substrates.

To evaluate what other potential functions of KDM5A may be affected by K1063 methylation, we incubated recombinant KDM5A 1 to 1090 enzyme methylated *versus* mock methylated *in vitro* by SMYD2 with HEK-293T cell lysates and then immunoprecipitated KDM5A *in vitro* interacting proteins, which were identified by mass spectrometry analysis. This revealed that while over 90% of proteins were common interactors, a subset of interactions was unique to or preferred the methylated *versus* the unmethylated enzyme. Out of 2891 proteins identified, 1894 proteins were identified with high confidence (Fig. S2*B* and Data Set S1, tab High Confidence Mass Spec hits) and included 59% of published KDM5A physical interactors (Fig. S2*C*, and Data Set S1, tab Known interactors found), confirming earlier studies (46, 47). 153 were unique or preferred to bind to methylated KDM5A (KDM5A/control ≥2 by at least one negative control and ≥1.5 by the second negative control, by percent total abundance ratios), and 115 were unique or preferred binding to unmethylated KDM5A. (Data Set S1, tabs for methylated KDM5A preferred interactors and unmethylated KDM5A preferred interactors).

Among the 153 proteins that interacted uniquely/preferentially with SMYD2-methylated KDM5A *in vitro*, several functional groups were identified including: proteins involved in cell cycle regulation and DNA metabolic processes, RNA processing and ribosome biogenesis proteins, proteins involved in cytoskeletal organization and chromosome organization and in protein folding (Fig. 2*C* and Data Set S1 tab GO Methylated KDM5A binders). In contrast, the 115 proteins that uniquely or preferentially interacted with 'unmethylated' KDM5A were significantly enriched in proteins involved in mitotic regulation, proteins activated during DNA damage and distinct proteins acting on RNA metabolism (Fig. 2*D*, and Data Set S1, tab GO Unmethylated KDM5A binders). Specifically, comparison of the methylated *versus* unmethylated KDM5A interactomes revealed that upon methylation by SMYD2, KDM5A gains interactions *in vitro* with IDH2 (the enzyme that produces KDM5A's co-substrate alpha-ketoglutarate) and TXNL1, both involved in redox balance, with BMS1, RPS15A part of the 40S ribosomal subunit, and NOP56, essential for ribosome biogenesis and translational fidelity, with CDK2, key cell cycle regulator, and with RNASEH2A, HPRT1, and DYNC1H1, which have roles in DNA repair, nucleotide homeostasis and cell division, respectively (Fig. 2*E*, left panel and Data Set S1). Multiple other proteins had also gained or increased interactions with methylated KDM5A including a subset involved in actin/microtubule/cytoskeleton (AGTPBPN1, ANLN, MAP4, and TNIK) and TTC4 which has chaperone activity (Fig. 2*E*, right panel). Conversely, upon methylation by SMYD2 *in vitro*, KDM5A loses, among others, its established interaction with WDR5 (36, 46, 47), thus potentially also weakening KDM5A-COMPASS complex interactions (Fig. 2*F* and Data Set S1) (37, 38). Methylated KDM5A also has decreased interactions with proteins involved in mitotic regulation including TUBB, with mitochondrial proteins involved in energy production and translation (EARS2, PRORP, NDUFS7, and MCCC2) with proteins essential for ribosome function, protein folding and degradation (RRP9, RRP15, EIF2B4, TXNDC5, PSMD14) and with transcriptional regulators/chromatin organization proteins (WDR5 previously mentioned, PRCC, CBX3) and cell cycle/DNA repair regulators (CHEK1, MPG) (Fig. 2*F* and Data Set S1). Altered interactions upon *in vitro* methylation of KDM5A by SMYD2 were validated by Western blotting of WDR5 and TUBB in KDM5A immunoprecipitates (Fig. S2*D*), confirming mass spectrometry results. Thus KDM5A methylated by SMYD2 has lower enzymatic demethylase activity and partly altered protein interaction partners *in vitro*.

Mutant K1063A KDM5A shows enhanced global demethylase activity in cells

Having established that KDM5A methylated by SMYD2 has lower histone demethylation capacity, we next evaluated the effects of mutating K1063 on KDM5A, at the site of SMYD2 methylation. The engineered K1063A KDM5A mutant (MUT) was expressed at equivalent levels as the WT KDM5A (Fig. 3*A*) in HCT116 cells knocked out for endogenous KDM5A expression (Fig. S3*A*). When the knockout cells were reconstituted with the K1063A MUT, they exhibited enhanced histone demethylase activity, being more efficient in removing H3K4me3 than the cells reconstituted with equivalent levels of the WT KDM5A (Fig. 3, *A* and *B*), as quantified over multiple Western blot experiments measuring cellular H3K4me3 global levels (Fig. 3*B*) with equivalent expression of WT or MUT KDM5A (Fig. 3*A* and Fig. S3, *B*–*C*).

We then directly measured H3K4me3 by ChIP-seq to identify the sites of H3K4me3 demethylation in the knockout cells reconstituted with the WT *versus* the MUT KDM5A. Consistent with the Western blot results shown above, we found that the cells expressing MUT KDM5A showed significantly lower levels of H3K4me3 (globally, Fig. 3*C* and at specific genomic elements, Fig. S3*D*), indicative of the higher demethylase capacity of the MUT enzyme, which was expressed at equivalent levels as the WT (Fig. 3*A* and Fig. S3, *B*–*C*). This higher demethylase activity of the MUT is exactly the opposite phenotype of the KDM5A methylated by SMYD2 at K1063, which showed lower demethylase activity (see Fig. 2, *A* and *B*).

When we examined the sites of H3K4me3 demethylation across the genome, comparing the action of exogenous WT *versus* MUT KDM5A, we observed a redistribution of demethylated peaks across the genome. Analysis of H3K4me3 ChIP-seq data indicated that there is a set of loci uniquely demethylated by the WT KDM5A, a common set of loci

buffer) *versus in vitro* methylated KDM5A 1 to 1090. Unmethylated KDM5A values are an average of the two controls ± SEM where the averages were set to 1. For graphing clarity, all values were multiplied by a common factor and are thus relative. Examples of interactions gained by methylation are shown in panel (*E*) and lost by methylation of KDM5A are shown in panel (*F*).

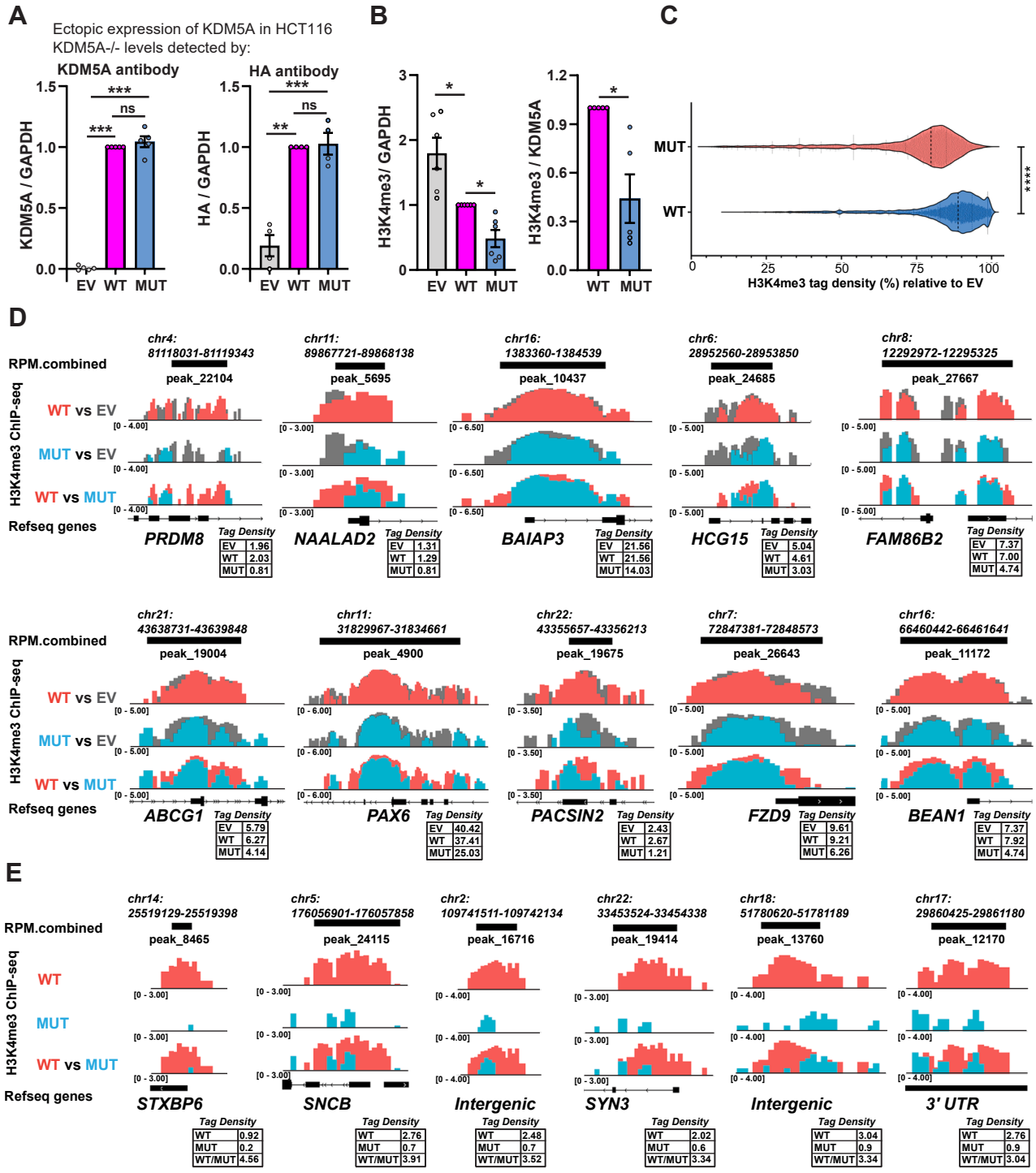

Figure 3. KDM5A K1063A has higher demethylase activity than WT. *A*, ectopic expression of KDM5A protein levels assessed by Western analysis using anti-KDM5A (*left*, n = 5) or HA (*center*, n = 4) antibodies, normalized to GAPDH. Western blots are shown in Fig S3, *B* and *C*. *B*, H3K4me3 levels in cells, *left*: normalized to GAPDH (n = 6), *right*: normalized to KDM5A (n = 5) assessed by anti-KDM5A antibody. See also Fig S3, *B* and *C*. (*A*, *B*) *p*-values are from Welch test, 2-tailed, unequal variance. *, $p \leq 0.05$, **, $p \leq 0.01$,***, $p \leq 0.001$, ns, not significant. *C*, violin H3K4me3 tag density profile plots for all peaks identified by ChIP-seq analysis that have EV tag density equal to or higher than WT (EV ≥ WT). Plotted values correspond to % H3K4me3 tag density in WT *versus* MUT relative to EV for each Chip seq peak. Median values (*thick dotted lines*) and quartiles (*thin dotted lines*) for each distribution are depicted within the plot. Statistical significance was determined using two tailed *t* test (nonparametric, Mann-Whitney test). *p* value < 0.0001 (****). Plots demonstrate an overall decrease in global levels of H3K4me3 enrichment in the MUT compared to WT indicating the higher demethylase activity of the MUT KDM5A. KDM5A protein levels in EV, WT and MUT samples are shown in Figure S3*C*. *D–E*, IGV genome browser visualization of H3K4me3 enrichment across samples, graphed in log scale as indicated for each peak. Inset tables display the corresponding tag densities for the peak in each of the three samples. Genomic coordinates (RPM-combined) are indicated for each region visualized. *D*, genome tracks for promoter_TSS regions of select candidate genes that demonstrate decreased H3K4me3 enrichment specifically in the MUT group compared to WT and EV. Featured promoters demonstrate a selection of the highest fold difference in tag density between the WT and MUT groups (WT/MUT ≥ 1.2 and EV/WT ≥ 0.9 & ≤ 1.1) among all identified MACS peaks in the ChIP seq analysis. *E*, overlay of sample H3K4me3 tracks in WT *versus* MUT transfected HCT116 KDM5A−/− cells at the indicated genomic regions demonstrating greater than three fold tag density values in WT compared to MUT.

demethylated to a similar extent by both the WT and MUT, and a large set of loci that are specifically decreased by MUT KDM5A (Data Set S2). A greater number of loci were exclusively or more robustly demethylated by the MUT enzyme (MUT H3K4me3 levels decreased by at least 1.5 fold at 4173 peaks) compared to the WT (3697 peaks decreased by at least 1.5) (Supplementary Data Set S2, tab EVover MUT ≥ 1.5 and EV over WT ≥ 1.5), again indicating the higher demethylase activity of the MUT. Among the MUT unique demethylated loci (Data Set S2, tab MUT unique ChIP-seq_425peaks and Fig. S3*E*) were multiple TSS regions, which demonstrated decreased H3K4me3 levels exclusively in the presence of MUT but not WT KDM5A (Fig. 3*D*).

Genomic annotation analysis of the peaks exclusively or 2 to 3 fold more robustly demethylated by MUT KDM5A *versus* WT revealed regions preferentially demethylated by the MUT or excluded from its action. Among the H3K4me3 peaks found decreased only in the presence of the KDM5A K1063A mutant (WT/MUT≥3, 652 peaks) (see examples in Fig. 3*E*) we found an over-representation of peaks in intergenic regions (Simple repeats/SINE/Alu/LINE, LTR regions, and other intergenic sequences) and in introns along with a decrease of promoter TSS, 5′UTR and CpG island regions, compared to the annotation of sites which are equally acted upon by WT and MUT (11,647 peaks), as shown in Figure 3*E* and Table 1, left side. This pattern remains generally valid (MUT demethylated peaks enriched in intergenic regions and introns and depleted in TSS, 5′UTR and CpG islands) also when we compare the peaks on which both the WT and the MUT enzymes act similarly and by two fold reduction of tag densities *versus* the sites in which the WT does not act but the MUT is active and decreases tag densities by at least two fold (Table 1, right side).

MUT unique demethylated peaks (defined as EV/WT 0.9–1.1 fold and WT/MUT ≥ 1.5 fold per tag density ratios, 425 genes) corresponded according to HOMER, to genes over-representing ToppGene biological pathways for export from cell (GO:0140352), cell to cell signaling (GO:0007267) and regulation of secretion (GO:1903530) (Fig. S3*F* and Data Set S2, tabs MUT unique_ChIP seq_425 peaks and MUT Unique_ChIPseq_GO Analysis). Thus, MUT KDM5A exhibits increased global H3K4me3 demethylase activity and acts at new genomic sites compared to the WT enzyme.

Overactive K1063A KDM5A acquires new transcriptional gene targets

To understand the functional consequences of MUT KDM5A enhanced activity, we expressed WT or K1063A KDM5A at equivalent protein levels in HCT116 KDM5A−/−cells (Fig. S4*A*) and assessed gene expression profiles by RNA-seq. This showed 319 genes upregulated by WT KDM5A (WT/EV ≥ 1.5) and 721 downregulated genes (WT/EV ≤ 0.67) (Data Set S3). Expression of the MUT KDM5A upregulated 621 genes (MUT/EV ≥ 1.5), about twice the number of genes upregulated by WT, and downregulated 3303 genes (MUT/EV ≤ 0.67), about 4 to 5 times the number of WT downregulated genes (Data Set S3). In addition, the fold change in expression was generally greater in MUT-regulated genes. Thus, by both the number of genes affected as well as by fold change, K1063A KDM5A had wider and stronger effects on transcription than WT KDM5A (Fig. 4*A*). As expected, both WT (721 down and 319 up) and MUT (3303 down and 621 up) enzyme expression caused more genes to be downregulated than upregulated, consistent with direct transcriptional repression effects through the removal of H3K4me3. WT and MUT shared 15% ≥ 1.5 fold upregulated and 14% ≤ 0.67 downregulated gene targets (Fig. 4*B* and Fig. S4*B*).

Among the 539 genes whose expression was downregulated uniquely by K1063A KDM5A but not down-regulated by WT KDM5A (MUT/EV ≤ 0.67 and WT/EV 0.9–1.1 fold, Data Set S3, tab MUT unique down-regulated) were a set of genes involved in lipid metabolism, negatively affecting essential cell

Table 1

Comparison of genomic annotations associated with different categories of H3K4me3 peaks in WT *versus* MUT KDM5A expressing HCT116 KDM5A−/− cells

Detailed annotation	WT/MUT ≥ 3.0	%	WT/MUT 0.9–1.1	%	Flsher's exact test *P* value	Significance	EV/WT0.9–1.1 & WT/MUT ≥ 2.0	%	EV/WTOR EV/MUT ≥ 2. 0 & WT/MUT0.9–1.1	%	Fisher's exact test *P* value	Significance
Repeat elements	141	21.6	1104	9.5	<0.0001	****	24	17.8	55	15.6	0.58	ns
LTR	55	8.4	284	2.4	<0.0001	****	6	4.4	16	4.5	>0.9999	ns
hATTransposons	9	1.4	67	0.6	0.02	*	3	2.2	3	0.8	0.35	ns
Low complexity	2	0.3	34	0.3	0.7163	ns	1	0.7	0	0.0	0.28	ns
CpG	24	3.7	1754	15.1	<0.0001	****	5	3.7	48	13.6	0.00	**
Promoter_TSS	29	4.4	3209	27.6	<0.0001	****	6	4.4	61	17.3	0.00	***
TTS	12	1.8	227	1.9	>0.9999	ns	2	1.5	7	2.0	>0.9999	ns
Exon	14	2.1	639	5.5	<0.0001	****	4	3.0	19	5.4	0.34	ns
Intron	181	27.8	2320	19.9	<0.0001	****	35	25.9	62	17.6	0.04	*
3′UTR	9	1.4	59	0.5	0.01	RR	1	0.7	3	0.8	>0.9999	ns
5′UTR	7	1.1	488	4.2	<0.0001	****	0	0.0	19	5.4	0.00	**
Intergenic	162	24.8	1172	10.1	<0.0001	****	48	35.6	57	16.1	<0.0001	****
Non-coding	6	0.9	233	2.0	0.06	ns	0	0.0	3	0.8	0.56	ns
Other	1	0.2	57	0.5								
Total peaks	652	100	11,647	100		.	135	100	353	100		

H3K4me3 ChIP seq peaks from EV, WT and MUT were filtered based on their tag densities as indicated and annotated using HOMER. Individual annotations for Simple_repeat, SINE|Alu, L2a|LINE|L2 were grouped together and presented as "Repeat elements". Annotations for AT_rich, CT-rich, C-rich Low_complexity were grouped and presented as "Low_complexity". Total number of peaks within each annotation term and their percentages were compared using various filtering criteria and their statistical significance determined using Fisher's exact test (two sided, *, $p < 0.05$; **, $p < 0.01$; ***, $p < 0.001$; ****, $p < 0.0001$, ns = not significant).

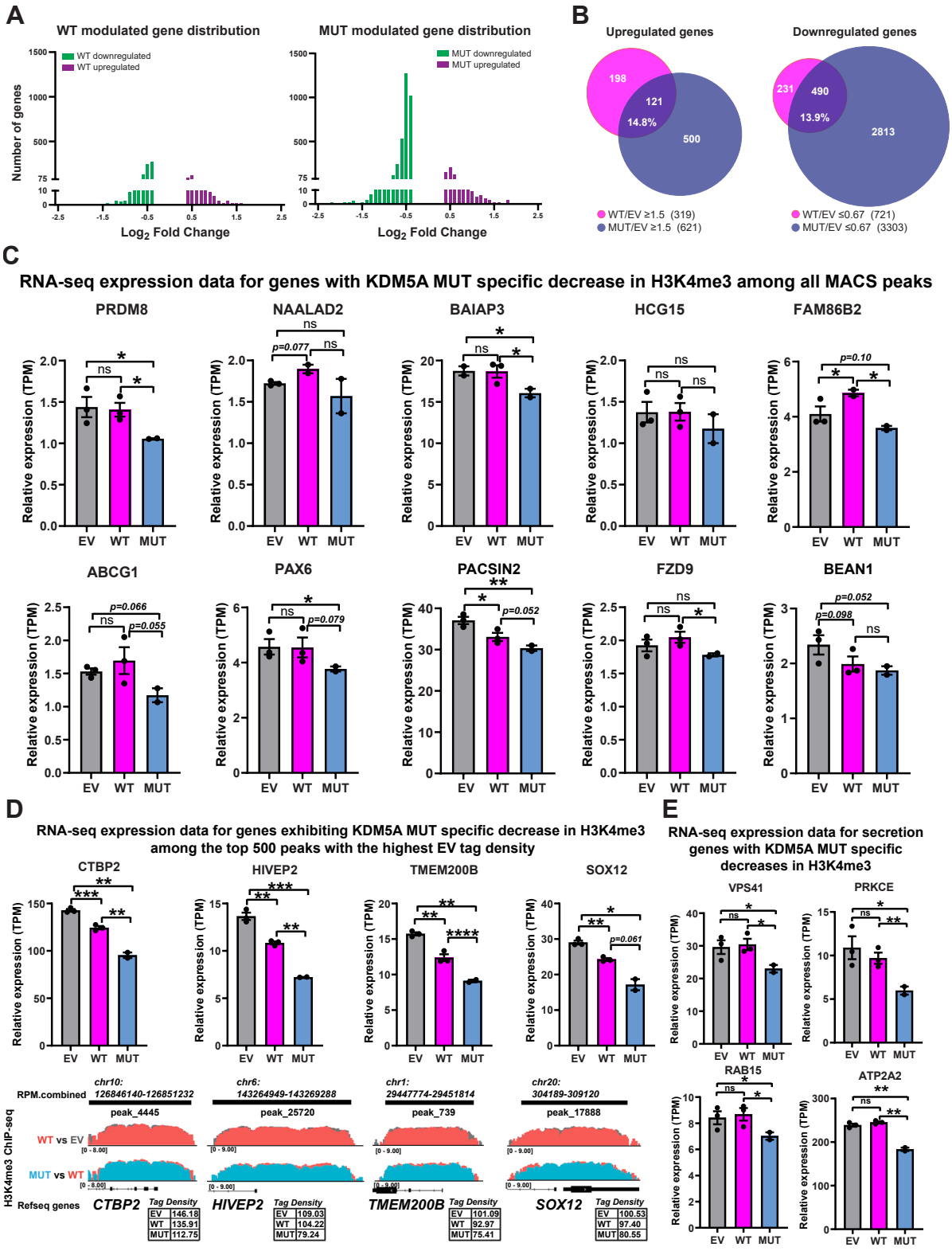

Figure 4. MUT KDM5A modulates new transcriptional gene targets. *A*, RNA-seq data from EV, WT, and MUT conditions were analyzed for differential gene expression. Fold-change ratios (WT/EV and MUT/EV) were $\log_2$-transformed and plotted as histograms with 0.1 bin sizes. Upregulated and downregulated genes were defined by fold-change thresholds of ≥1.5 and ≤ 0.67, respectively. KDM5A was excluded from both plots due to its high exogenous expression. *B*, Venn diagrams displaying common and unique upregulated or downregulated genes upon re-expression of WT or MUT KDM5A in HCT116 KMD5A−/− cells. *C–E*, normalized (TPM, Transcripts per million) gene expression levels from RNA-seq analysis for candidate genes in HCT116 knockout cells expressing empty vector (EV), KDM5A wild type (WT) or KDM5A mutant (MUT) constructs. *C*, expression levels for the ten candidate genes shown in Figure 3, selected based on decreased H3K4me3 enrichment specifically in MUT compared to EV and WT from all MACS peaks. *D*, gene expression levels and H3K4me3 genome track overlays for select promoter_TSS regions that demonstrate decreased H3K4me3 enrichment specifically in MUT but not WT samples, identified among the 500 MACS peaks with the highest tag density in EV. *E*, relative gene expression for candidate genes that

growth pathways including phospholipid/glycerolipid metabolism (Fig. S4*C*, top panel). More generally, the genes whose expression was downregulated by MUT enzyme *versus* EV overrepresented chromatin remodeling, regulation of transcription by RNA Pol II, Wnt signaling genes and target genes of a number of transcription factors/co-regulators with roles in transcriptional control and cell growth/proliferation, including p300, E2F2, FOXO4, SKIL and RYBP (Fig. S4*C*, bottom panel and Data Set S3, MUT *versus* EV tabs).

We then analyzed the expression of the subset of genes that had been identified by ChIP-seq above to harbor MUT specific decreases in H3K4me3 peaks, including those highlighted earlier in Figure 3*D*. There was a general down regulation of gene expression at the 24 h time point post ectopic expression, consistent with the decreased levels of H3K4me3 mediated by the MUT but not the WT KDM5A at these and other functionally relevant sites of MUT-specific H3K4me3 decreases (Fig. 4, *C–E* and Fig. S4, *D–E*) including export from cell (GO:0140352) and cell-cell signaling (GO:0007267) (Fig. S3*F*).

Taken together, the MUT KDM5A alters gene expression more robustly than WT and acts to downregulate new transcriptional targets, including those that had been characterized as having MUT -pecific decreases in H3K4me3 levels by ChIP-seq. Thus, overall, K1063A KDM5A has enhanced demethylase activity on histones and on the genome and has an expanded set of transcriptional targets as established by the multiple approaches described above. Given that the MUT enzyme decreased the expression of genes essential to growth and cellular energy pathways, as shown above, we next assessed MUT KDM5A's effect on cellular proliferation.

Mutant KDM5A K1063A blocks cell proliferation, downregulates cell proliferation genes and exhibits expanded protein-protein interactions

To assess the functional significance of K1063A KDM5A on cell growth, we reconstituted HCT116 KDM5A−/−cells with equivalent levels of WT or MUT enzyme (Fig. S3*B* samples annotated "from proliferation assays") and measured proliferation over time. Strikingly, cells expressing MUT KDM5A, which has enhanced demethylase activity, reproducibly showed decreased cell number (Fig. 5*A*). Consistent with this result, HCT116 KDM5A−/− cells expressing MUT KDM5A showed decreased percent in S-phase and increased subG1 compared to cells expressing the equivalent levels of exogenous WT KDM5A (Fig. 5*B*). Thus, KDM5A, which cannot be modified at K1063, lowers global H3K4me3 levels more robustly than WT, decreases gene expression of new transcriptional targets, and leads to defects in cell growth.

To evaluate if KDM5A directly regulates cell cycle genes that could impinge on this proliferation phenotype, we analyzed existing KDM5A ChIP-seq data from HCT116 cells (39), and overlapped these target genes with H3K4me3 profiles of MUT specific plus MUT enhanced H3K4me3 peaks that showed decreased H3K4me3 levels *versus* WT (EV/WT 0.9–1.1 and WT/MUT ≥ 1.2, 1903 genes, 1905 peaks plus EV/WT ≥ 1.2 and WT/MUT ≥ 1.2, 1344 genes, 1350 peaks, Data Set S4). Of these 3247 genes acted on by the MUT, 290 overlapped with KDM5A direct targets (Data Set S4, tab 290). GO analysis of these 290 genes demonstrated enrichment in cell cycle regulatory genes and DNA metabolic process genes (Fig. 5*C*, Data Set S4, tab GO genes). KDM5A RNAseq analysis uncovered the transcriptional downregulation of a subset of these cell cycle regulatory genes which are indeed specifically or more robustly repressed by expression of the MUT *versus* the WT enzyme, concomitant with decreases in H3K4me3 near sites of KDM5A binding (Fig. 5*D*). Indeed, overall, expression of the MUT led to downregulation of 37.5% of KDM5A target genes within 24 h in the KDM5A−/− cells, while the WT enzyme downregulated less than 10% of KDM5A target genes in the same time (Fig. S5, *A–B* and Data Set S3, tab RNAseq_KDM5A targets_ALL).

We next examined the protein-protein interactions of the MUT KDM5A compared to WT enzyme. Mass spectrometry of HA-tagged KDM5A immunoprecipitated complexes (WT OR MUT) identified common and unique interacting proteins. Overall, 1683 proteins were identified with high confidence with a percent abundance greater than background samples expressing empty vector control. Of the known interactors of KDM5A previously reported (46, 47), 43% were present in our high confidence hits (Fig. 6*A*, Data Set S5, tab Known interactors found), which included not only nuclear but also some mitochondria and cytoplasmic proteins consistent with prior KDM5A studies (40–42).

We found that 1354 proteins interacted above EV background with WT and 1394 with MUT KDM5A, with 1064 being common to both (including HDAC2 and MORF4L2), and 290 unique to WT, including SMYD2 (Data Set S5, tab WT KDM5A proteome), while 329 were unique to MUT (Fig. 6*B*, Data Set S5, tabs WT KDM5A proteome or MUT KDM5A proteome). Among the common 1064 interactors, 256 proteins had 2-fold or greater abundance in the MUT *versus* the WT immunoprecipitated samples (Data Set S5, tab Unique & Preferred MUT KDM5A binders). The 290 WT unique interactors included known interactors such as MED1, and over-represented proteins corresponding to genes in three main processes, according to GO analysis: 1) ribosome biogenesis, RNA metabolism, 2) mitochondrial respiration, ATP production, and NAD(P)H metabolism, 3) ribonucleotide synthesis and regulation of mitotic phase (Fig. S6*A*, top panel and Data Set S5, tab GO Unique WT KDM5A binders). Interestingly, the 329 MUT unique interactors included

demonstrate significantly lower expression in MUT compared to EV and WT identified from top enriched biological processes, export from cell (GO:0140352) and cell-cell signaling (GO:0007267). Genes corresponding to H3K4me3 peaks exhibiting a tag density of at least 1.5 fold lower in MUT compared to WT while demonstrating comparable tag densities between EV and WT (EV/WT fold between 0.9–1.1 AND WT/MUT fold ≥1.5) were subjected to gene ontology analysis. *C–E*: Gene expression values are averages of indicated individual data points from RNA-seq analysis, with error bars representing SEM. n = 3 (EV), 3(WT), 2(MUT) unless mentioned. *p* values were calculated by one tail *t* test (*$p \leq 0.05$, **$p \leq 0.01$, ***$p \leq 0.001$, values are indicated for significance between 0.05 and 0.1). ns = not significant with $p > 0.1$.

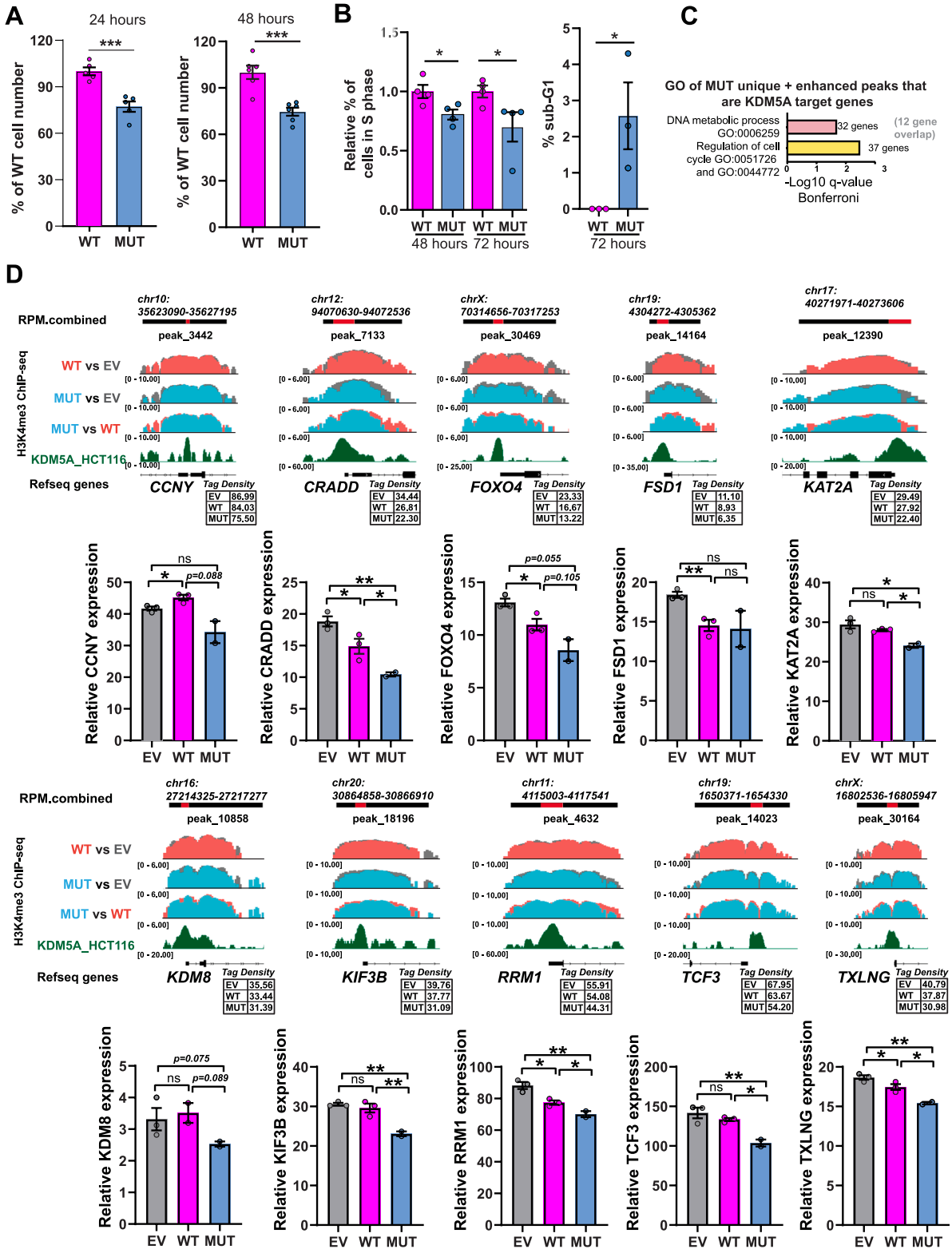

Figure 5. MUT KDM5A triggers blunted cell growth. *A*, cell number is reduced when mutant KDM5A is expressed compared to wild type after 24 (*left*, n = 5 of one experiment) or 48 (*right*, n = 3 per experiment for two individual experiments) hours of transfection. *p*-values are from Welch test, 2-tailed, unequal variance. *, $p \leq 0.05$, **, $p \leq 0.01$,***, $p \leq 0.001$, ns, not significant. *B*, relative percent number of cells in S phase (*left*) in WT *versus* mutant KDM5A expressing cells 48 and 72 h after transfection. Data are mean ± SEM, n = 4 for all samples and time points. The *right panel* shows the percent subG1 population. Data are mean ± SEM, n = 3. In both panels, *p*-values are *t* test, 1-tailed, unequal variance. *, $p \leq 0.05$. *C*, top significant GO terms over-represented in the MUT unique + MUT enhanced demethylated H3K4me3 peaks that are associated with direct KDM5A binding. *D*, gene expression profiles and corresponding ChIP-Seq H3K4me3 and KDM5A track overlays for cell-cycle regulatory genes featured in the mutant-specific (EV/WT 0.9–1.1 and WT/MUT ≥ 1.2, 1903 genes, 1905 peaks) and mutant-enhanced (EV/WT ≥ 1.2 and WT/MUT ≥ 1.2, 1344 genes, 1350 peaks). These 3247 genes were overlapped with HCT116 ChIPseq 5A targets for a total of 290 common on which we did GO. The top four-fifths biol processes were cell cycle

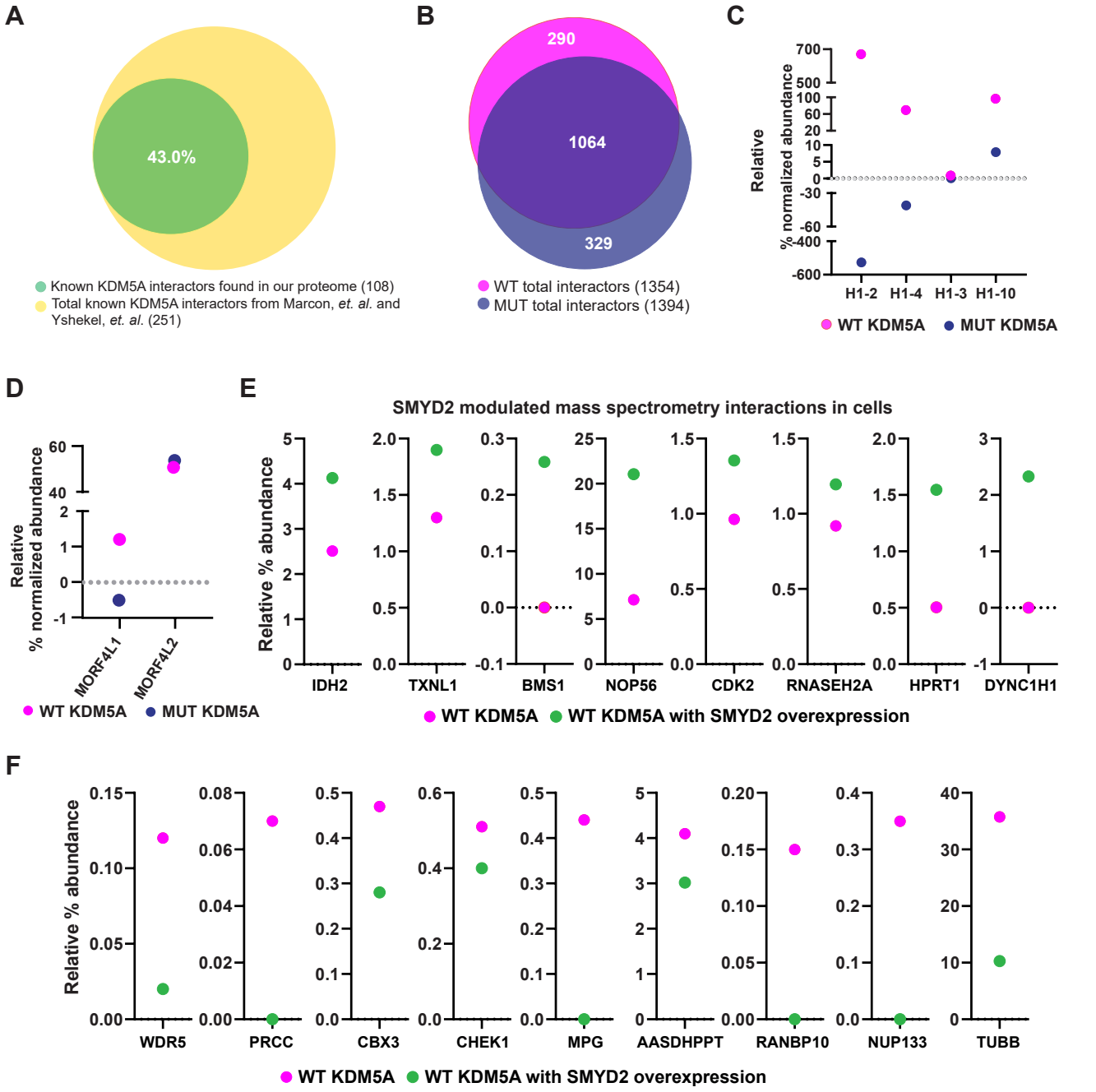

Figure 6. *In vivo* KDM5A interactome is sensitive to the K1063A mutation and to SMYD2 overexpression. *A*, venn diagram showing the percent of established KDM5A interactors that were also identified in cells in this study. *B*, venn diagram depicting the overlap of WT and MUT KDM5A interactomes in cells as measured by mass spectrometry. *C* and *D*, relative percent total abundance of select proteins of functional interest that interacted with WT *versus* MUT KDM5A in cells by mass spectrometry analysis. *E* and *F*, relative percent total abundance of select proteins of functional interest across several categories that interacted WT KDM5A in a SMYD2-dependent manner in cells as measured by mass spectrometry analysis. These interactions were also observed to be KDM5A methylation dependent *in vitro* as shown in Figure 2.

proteins whose genes are in similar GO terms, including RNA processing/translation and ribonucleotide binding/cell cycle but lacked mitochondria respiration/ATP production as a significant term and instead included chromosome organization (Fig. S6*A*, middle panel, and Data Set S5, tab Unique MUT KDM5A binders). When the MUT unique plus MUT enhanced (MUT/WT ≥ 2-fold interactors were considered together (329 + 256)), there was still no

(GO:0010564, Go:0051726, GO:1901990 and GO:0044772), so we combined these four and got 56 unique genes of which we chose these 10 based on RNAseq and IGV profile. The remaining GO term was DNA metabolic process GO:0006259. All five were Bonferroni significant. One tail *t* test results (unpaired with Welch's correction) are presented here. n = 3(EV), 3(WT), 2(MUT) unless mentioned. Criteria for significance: *p* values between 0.05 and 0.1 are mentioned instead of a "ns" notation. *p* values above 0.1 are marked "ns".

enrichment of mitochondria respiration/ATP production proteins, but there was significant enrichment of a new category related to protein folding and chaperones which included multiple heat shock proteins which have been reported previously as KDM5A interactors (Fig. S6*A*, bottom panel and Data Set S5, tab GO Unique & Preferred MUT KDM5A binders). Of note, we found that multiple isoforms of the linker histone H1 interacted with the WT but not the MUT KDM5A in cells (Fig. 6*C*). This result points to a potential way in which the actions of WT KDM5A may be more restricted on the genome *versus* the actions of MUT, which lacks or has weaker interactions with H1 isoforms (Fig. 6*C*). In addition, while both WT and MUT interact with MORF4L2, only WT interacts with MORF4L1 (Fig. 6*D*), suggesting the MUT has partly defective interactions with the Sin3/NuA4 acetylation complex and/or the PALB2 DNA repair complex (46, 47).

Thus, by H3K4me3 demethylation, by transcriptional effects as well as by protein-protein interactions, the MUT KDM5A has wider action on the genome, more robustly modulates cell cycle gene expression, has an altered interactome and functionally decreases cell proliferation, compared to the WT enzyme.

To further understand the impact of KDM5A interactions as modulated by SMYD2 methylation, we also identified by mass spectrometry proteins that interact with WT KDM5A in the context of SMYD2 overexpression in cells (see Western blot in Fig. S6*B*). Overexpression of SMYD2 altered the KDM5A interactome in cells with 211 interactors gained and 249 lost above background controls (Data Set S5, tab WT KDM5A + SMYD2 proteome). Importantly, multiple of the methylation-sensitive interactions that we had observed *in vitro* (Fig. 2, *E* and *F*) were confirmed here *in vivo*. Examples include the enhanced interaction of WT KDM5A in cells overexpressing SMYD2 with IDH2, TXNL1, BMS1, NOP56, CDK2, RNASEH2A, HPRT1, and DYNC1H1 (Fig. 6*E*) which we had already observed *in vitro* as methylation specific (see Fig. 2*E*, left panel). Conversely, proteins that we had observed lost interaction with *in vitro* methylated KDM5A (Fig. 2*F*) were seen to also have decreased interactions with KDM5A in cells overexpressing the SMYD2 methyltransferase (Fig. 6*F* and Fig. S6*C*). Of particular interest was the finding that while the WT KDM5A enzyme without SMYD2 overexpression interacted with WDR5, as we had seen earlier with the unmethylated KDM5A in Figure 2*F* and Figure S2*D*, this interaction of WT KDM5A with WDR5 was also decreased upon SMYD2 being overexpressed in cells (Fig. 6*F*). This independent result underlines that upon methylation by SMYD2 (*in vitro* in Fig. 2*F* and Fig. S2*D*, or in cells here in Fig. 6*F*), KDM5A has weaker or no interactions with WDR5 likely therefore affecting its interactions with the COMPASS complex. Similarly, KDM5A interactions with a number of other proteins involved in chromatin remodeling, cell cycle regulation, ribosome function and energy generation were also decreased in the presence of SMYD2 overexpression (Fig. 6*F*) as was seen earlier for these same proteins with *in vitro* methylated KDM5A (Fig. 2*F*), consistent with the methylation-dependent nature of these interactions in cells. Of note, the known interactors MRPL23 and RPL23 (46, 47) which are essential components of the large ribosomal subunit in the mitochondria and cytoplasm, respectively, showed methylated-KDM5A dependent interactions with MPRL23 having weaker associations and RPL23 have stronger associations with methylated KDM5A both *in vitro* and in cells (Fig. S6*D*, left and middle panels). Furthermore, the basal transcriptional regulators MED1, MED17 and TAF9B, also previously reported to interact with KDM5A (47), likewise associated with KDM5A in a methylation-sensitive manner with opposite preference (MED1 and MED17 loose interactions upon SMYD2 overexpression whereas TAF9B gains KDM5A interaction) as can be seen in Figure S6*D*, right panel. These results, together with data presented in Figure 2, point to the methylation of KDM5A altering a subset of its protein interactors. Indirect effects, of course, cannot be fully discounted but are unlikely especially for the changes seen both with SMYD2 overexpression in cells (Fig. 6) as well as with *in vitro* SMYD2 methylation of KDM5A (Fig. 2 and Fig. S2).

Thus, KDM5A has altered interactions both when K1063 is mutated as well as when SMYD2 is overexpressed in cells or when KDM5A is methylated *in vitro* by SMYD2. These results indicate that a subset of the KDM5A interactome is modulated by SMYD2 methylation of this impactful KDM known to drive aspects of cancer and neurodegenerative disorders.

Discussion

The Jumonji demethylase KDM5A has wide-ranging biological functions affecting the epigenome, the transcriptome and even the proteome. Here we have established that the activity of KDM5A is modulated by methylation by SMYD2 *in vitro* and in cells, leading to altered demethylase activity, gene expression and protein-protein interactions. Several implications of both mechanistic and translational significance can be extracted from this work. First, that a single PTM or a mutation in a modified lysine can have robust effects on KDM5A's demethylation capacity, resulting in changes in both the extent and the sites of genomic H3K4me3 demethylation, with the corresponding changes in gene expression patterns. Secondly, that the KDM5A proteome is methylation-sensitive with some interactors of established functional significance as well as new interactors identified here, associating uniquely or more strongly with either the methylated or the unmethylated form of KDM5A. Third, that among the genomic targets and the protein interactors that are methylation sensitive, there are many of disease significance including cancer-related and neurological disorder-related genes or proteins.

In relation to KDM5A-containing complexes, we found that WDR5, MED1, and MED17 associate preferentially with the unmethylated form of KDM5A or with KDM5A in the absence of SMYD2 overexpression, suggesting that methylated KDM5A loses or has weaker interactions with the COMPASS and the MEDIATOR complexes, respectively. In

contrast, TAF9B associated more strongly with KDM5A when SMYD2 was overexpressed indicating differential complex formation with the basal transcriptional machinery. These altered associations can potentially have far-reaching effects not only on transcriptional control but also on genomic stability and cellular signaling, and on re-replication and local copy gains (25, 38, 43, 48). In this regard, it is interesting that K1063 is within the F6 fragment of KDM5A (aa1031–1250 which contains PHD2) found by the Miller laboratory to be moderately PARylated during the DNA damage response (43). In line with this observation, we found that KDM5A and SMYD2 have common genomic targets which include a large proportion of BRCA2 target genes, some of which show marked decreases in H3K4me3 levels and in gene expression in a MUT-selective manner (Data Set S3, tab "399 KDM5A SMYD2 common_RNA-seq" and Data Set S4, tab "MUTunique&enhanced demethylated"). Among the methylation-dependent interactors were also several proteins associated with neurological disease (47, 49, 50), including MED17 mentioned above and CTBP1 and TAF4 (which had increased interaction with *in vitro* methylated KDM5A), indicating that KDM5A may have methylation-sensitive partners also in these disorders.

The decreased cell proliferation of knockout cells reconstituted with equivalent protein levels of the K1063A MUT *versus* the WT KDM5A enzyme illustrates the cumulative effects of the MUT enzyme, which has higher histone demethylase activity *in vitro* and in cells, and more robustly lowers H3K4me3, repressing transcription more strongly and at new targets. Although these effects were clearly seen in the HCT116 KDM5A−/− cells reconstituted with the K1063A mutant KDM5A and not with WT, it is possible, yet unlikely, that other KDM5 family members may be differentially compensating and contributing to these differences. The MUT-specific H3K4me3 demethylation and downregulation of KDM5A target genes involved in cell growth and cell cycle progression including CCNY, KIF3, RRM1 and TCF3/E2A may be partly responsible for this phenotype. In addition, our results suggest that MUT KDM5A may lead to defective energy production by differentially affecting both lipid metabolism and mitochondrial respiration, both functions of KDM5A which partly mediate its pro-growth effects (40, 41). Whether the effects of the MUT K1063A KDM5A are solely due to lack of methylation or also of other potential modifications or charge properties of K1063 remains an open question.

Of future potential interest, the interactome of "unmethylated" KDM5A included 115 proteins, 77 of which have been reported to be themselves methylated, with two of these being dimethylated on K and nine at R residues and one protein being trimethylated at K (Data Set S1, Methylation status of MS hits). In contrast, SMYD2-methylated KDM5A interacted with 153 proteins 123 of which have been found to be methylated with notably 16 of these containing dimethyl R and 11 proteins containing di- or trimethylated K (8 with dimethyl and 3 with trimethyl), including HSP90A, a known substrate of SMYD2 (33, 35, 51). These interacting methylated proteins, especially the di or trimethylated ones, may be potential substrates for demethylation by KDM5A and if so, this activity of KDM5A will likely also be regulated by methylation by SMYD2.

Taken together, this study establishes that a subset of the KDM5A interactome is modulated by SMYD2 methylation of at least K1063 and that this modification has measurable effects on the genomic H3K4me3 demethylase activity of KDM5A, on its transcriptional targets, on cell proliferation and on protein complex interactions, all of which play a role in KDM5A's impact on cancer and neurodegenerative disorders.

Experimental procedures

Reagents

Purified KDM5A protein (Flag-tagged, residue 1–1090 of hKDM5A expressed in insect cells) was commercially purchased from BPS Bioscience. KDM5A peptides were custom made by EZBioLab: KDM5A 222 wild type, NILPKRTRRVKTQSESGDVS; KDM5A 222 A, NILPKRTRRVATQSESGDVS; KDM5A 1063 wild type, WRERTGRTFLKKNSSHTLLQ, and KDM5A 1063 A, WRERTGRTFLAKNSSHTLLQ. DNA oligos were custom made by Sigma: pET11d Pml1, 5′-ATA TAT CAC GTG CAC AGA TGC TCT TCT TGC TTT-3′; pET11d Kpn1: 5′-ATA TAT GGT ACC GGC TGC TAA CAA AGC CCG AAA GG-3′; KDM5A WILD TYPE 1 to 1090 to 1, 5′-ATG GCG GGC GTG GGG CCG-3′; KDM5A WILD TYPE 1 to 1090 to 2, 5′-ATA TAT GGT ACC CTA CCT CCT ATT TTT GCC ACT CCC-3′; KDM5A MUT K1063A-1, 5′-GGC GGA CGT TTC TTG CGA AGA ATT CTA GCC ATA CAT TG-3′, and KDM5A MUT K1063A-2; 5′-CAA TGT ATG GCT AGA ATT CT TCG CAA GAA ACG TCC GCC-3′. Histone H3K4me3 (31,210) was purchased from Active Motif. KDM5A demethylase assay kit (Epigenase JARID Demethylase Activity/Inhibition Assay kit, P-3083) was purchased from Epigentek. Purified p53, SMYD2, and G9A proteins were generous gifts from Cheng-Ming Chiang's laboratory, UT Southwestern Medical Center. Purified histones were a generous gift from Bing Li's laboratory, UT Southwestern Medical Center. Zymo-Spin ChIP kit (D5210) was purchased from Zymo Research. *Mycoplasma* PCR detection kit (25,235) was purchased from Boca Scientific.The following reagents were purchased from Millipore-Sigma: ChIP-grade, validated rabbit anti-H3K4me3 (07–473), rabbit anti-H3K4me2 (07–030), rat anti-HA (1,867,423,001), mouse anti c-Myc (M4439), mouse anti-Tubulin (T5168), mouse anti-Flag (F1804), M2 beads (or anti-Flag beads, A2220), Flag peptide (F3290). Rabbit anti-JARID1A (876S), rabbit anti-beta tubulin (2128S), goat anti-rabbit IgG, HRP linked (7074) and goat anti-mouse IgG, HRP linked (7076) were purchased from Cell Signaling Technology. Mouse anti-H3 (39,763) was purchased from Active Motif. Rabbit anti-HA (ab9110), rabbit anti WDR5 (ab178410) were purchased from Abcam. Rabbit anti-JARID1A (A300–897A-M) was purchased from Bethyl, and mouse anti-GAPDH (GTX627408) was purchased from Gene Tex. Donkey anti-rabbit IgG (H + L) IRDye800 (P/N: 926–32213) and Donkey anti-Mouse IgG (H + L) IRDye680 (926–68072) were purchased from LI-COR. Normal rabbit IgG

(sc2027), mouse anti-SMYD2 (sc-393827) and mouse anti-cyclophilin F (sc-376061) were purchased from Santa Cruz. Rabbit anti-mono/di methyl lysine (PTM Bio, PTM-602) was purchased from PTM BIO, and goat anti-Rat, HRP linked (A1277–5) was purchased from BioVision. The cyclophilin antibody used for loading control was purchased from Abcam (ab236760). All antibodies used in this study were validated for the application used by the manufacturer and passed our laboratory specificity checklist including clear bands at the expected molecular weight, loss of signal upon knockout of the target protein, increased signal upon overexpression and generally robust signal over background. When applicable, dot blots with purified protein or peptides were also used to confirm specificity such as for the antibodies detecting specific histone methylation levels.

Biological resources

HCT116 parental (HD-PAR-073) and HCT116 KDM5A−/− (HD 104–105) were purchased from Horizon. HEK-293 T was obtained from James Brugarolas' laboratory, UT Southwestern Medical Center. pCAG-SMYD2-cMyc was a gift from Xiaobing Shi's laboratory, MD Anderson Cancer Center. pGFP was a gift from James Kim's laboratory, UT Southwestern Medical Center. pcDNA3.1myc-His(−) A was from Invitrogen. pcDNA3-HA-KDM5A was a generous gift from Dr Elizaveta Benevolenskaya, University of Illinois, College of Medicine.

Cell culture

HEK-293T cells were maintained in DMEM (Sigma, D5796) supplemented with 10% FBS. HCT116 parental (HD-PAR-073) and HCT116 KDM5A−/− (HD 104–105) were obtained from Horizon Discovery and maintained in RPMI-1640 (Sigma, R8758) supplemented with 5% FBS. Culture media for KDM5A−/− cells were further supplemented with 300 μg/ml G-418 (RPI G64000). Cells were maintained in a humidified environment at 37 °C with 5% CO_2. Cell line verification by DNA fingerprinting was carried out with the PowerPlex Fusion system (Promega, DC2408), enabling amplification and fluorescent detection of 23 short tandem repeat (STR) loci and Amelogenin, which collectively provide a genetic profile with a random match probability of 6×10^{-29}. Fingerprints were compared against our database of more than 2000 reference fingerprints collected from ATCC, DSMZ, JCRB, and RIKEN (52) and from our own internal resources (53). A match is called between two fingerprints when at least 80% of the alleles are identical according to the shared allele match algorithm defined by CLAC (International Cell Line Authentication Committee). Cells were periodically tested for *mycoplasma* using e-Myco *Mycoplasma* PCR Detection Kit (Boca Scientific, 25,235).

Plasmid construction

Plasmid constructs for bacterial expression of h*KDM5A* (amino acids 1–1090) were generated by amplifying h*KDM5A* cDNA corresponding to residues 1 to 1090 from pcDNA3-RBP2 (Addgene) using primer pair 5′-ATG GCG GGC GTG GGG CCG-3′ and 5′-ATA TAT GGT ACC CTA CCT CCT ATT TTT GCC ACT CCC-3′ to introduce KpnI restriction enzyme sites. Next, the expression vector pET11d (Novagen) was modified by introducing Pml1 and Kpn1 restriction enzyme sites by Polymerase Chain Reaction (PCR) using oligos, 5′-ATA TAT CAC GTG CAC AGA TGC TCT TCT TGC TTT-3′ and 5′-ATA TAT GGT ACC GGC TGC TAA CAA AGC CCG AAA GG-3′. PCR products for the modified pET11d and KDM5A cDNA were cleaved with the corresponding restriction enzymes and ligated to generate pET11d-Flag-KDM5A 1 to 1090. The KDM5A mutant version was generated by replacing Lysine (K) at 1063 with Alanine (A) using site-directed mutagenesis with primer pair K1063A: 5′-GGCGGACGTTTCTTGCGAAGAATTCTA GCCATACATTG-3′ and 5′-CAATGTATGGCTAGAATT CTTCGCAAGAAACGTCCGCC-3′ and KDM5A WT construct as template.

The full-length h*KDM5A* (amino acids 1–1690) construct for mammalian expression was generated in two steps. First, the vector pcDNA3.1 was modified to remove a RsrII restriction enzyme site and ligated to Xba1 and Kpn1 digested KDM5A fragment (1–1090 or 1–1090 K1063A) obtained from pET11d KDM5A constructs, resulting in pcDNA3.1-RsrII-Flag-KDM5A (1–1090) and KDM5A (1–1090) K1063A. In a second step, the coding sequence for amino acids corresponding to the C-terminal end of h*KDM5A* (amino acids 1091–1690) was generated by RsrII and KpnI restriction enzyme cleavage of pcDNA3-HA-KDM5A (generous gift from Dr Elizaveta Benevolenskaya, University of Illinois, College of Medicine). This fragment was subsequently introduced into pcDNA3.1-RsrII-Flag-KDM5A (1–1090) and pcDNA3.1-RsrII-Flag-KDM5A (1–1090) K1063A to generate pcDNA3.1-RsrII-Flag-KDM5A (1–1690, full-length KDM5A) and pcDNA3.1-RsrII-Flag-KDM5A (1–1690 K1063A, full length mutant KDM5A). As a final step, the Flag tag in both vectors were swapped with an HA tag, resulting in expression vectors, pcDNA3.1-HA-KDM5A (KDM5A WT) and pcDNA3.1-HA-KDM5A K1063A (KDM5A mutant, MUT), which were used in RNAseq, ChIP-seq and mass spectrometry experiments.

Transfections

HCT116 KDM5A−/− cells were plated at 5 to 6×10^5cells/well in a 6-well plate in antibiotic-free media. 24 h after seeding, cells were transfected with a mixture of 0.1 μg pGFP plasmid and 2 to 2.4 μg pcDNA3.1-HA-KDM5A (WT), KDM5A mutant (MUT) or the empty vector (EV) using Polyplus jetOPTIMUS DNA Transfection Reagent (Polyplus, 101000006) following the manufacturer's instructions. Transfected cells were incubated for 24 h and collected for analyzing KDM5A and H3K4me3 expression levels by Western blot analysis. To assess the effect of wild-type or mutant KDM5A on cell proliferation, the total number of cells was counted at the 24 h and 48 h time points post-transfection. For RNAseq and ChIPseq experiments in

HCT116 KDM5A−/− cells, scaled-up transfections were performed in 150 mm dishes.

For mass spectrometry analysis, HEK-293T cells were plated in 150 mm dishes at 5.5 × 10^6cells/plate and incubated overnight. Cells were transfected with empty vector (EV), wild-type *KDM5A* (WT) or mutant *KDM5A* (MUT) with a mixture of 1.6 μg pGFP plasmid and 30.4 μg of *KDM5A* (WT or MUT) and 4 μg of SMYD2 or its empty vector (to get the desired combination of over-expressing KDM5A alone or KDM5A with SMYD2) per 150 mm dish in 3.2 ml buffer and 32 μl transfection reagent using Polyplus jetOPTIMUS DNA Transfection Reagent kit (Polyplus, 101000051).

In vitro *methyltransferase assay*

Recombinant human KDM5A 1 to 1090 Flag-tagged (0.24 μM, BPS Bioscience, 50110), p53, purified histones or KDM5A peptides were incubated with recombinant SMYD2 or G9A (1.5 μM) in the presence of 5 μM Adenosyl-L-Methionine, S-[methyl-^{3}H] (PerkinElmer, NET155) in 53.3 mM Tris-HCl, pH 9.0, and 133.3 mM NaCl. The methylation reaction was carried out by incubating the reaction mixture at 30 °C for 2 h. A third of the methylation reaction mixture was spotted on P81 Whatman papers, washed 4 times using freshly diluted 50 mM $NaHCO_3$, pH 9.0, and dried overnight at room temperature. These filter papers were used to determine the incorporated ^{3}H count. The total ^{3}H counts were determined using the other one-third of the reaction mixture that was diluted and spotted on P81 Whatman paper and dried overnight without performing any washes on the filter paper. Total and incorporated ^{3}H-methyl counts were determined by placing the corresponding dried filters in 10 ml of Scintillation fluid (Universol, MP, 882480) using a Beckman LS6000TA Scintillation counter. The final ^{3}H incorporation was calculated as follows: % ^{3}H incorporation: [(incorporated count/total count) x (SAM μM) x 100]/ Substrate μM.The remaining reaction mixture was denatured in protein sample loading buffer (2x Laemmli sample buffer, 62.5 mM Tris-HCl pH 6.8, 2% SDS, 25% glycerol, 5% β-mercaptoethanol, 0.01% bromophenol blue), resolved on a 4 to 12% NuPage Bis-Tris gel (Invitrogen) using NuPAGE MOPS SDS Running buffer (NP0001, Invitrogen) at 150 V for 1 h. The gel was washed with water, stained with Coomassie Blue solution at room temperature for 1h followed by destaining steps with solution 1 (50% methanol, 10% acetic acid) for 10 min then with solution 2 (10% methanol and 7% acetic acid) overnight. After de-staining, the gel was washed extensively with water and then with amplified solution (NAMP100V, GE Healthcare) for 20 min. Gels were subsequently dried and exposed to an autoradiography film at −80 °C for 24 h to detect histone methylation and 72 h to detect KDM5A methylation.

Methylation of KDM5A peptides was performed in the same manner as methylation of recombinant KDM5A. The amino acid sequences of 20 amino acids encompassing residue 222 or 1063 of hKDM5A were custom synthesized by EZBioLab. The amino acid sequences are: 222 wild type, NILPKRTRRV**K**TQSESGDVS; 222 A, NILPKRTRRV***A***TQSESGDVS; 1063 wild type, WRERTGRTFL**K**KNSSHTLLQ; 1063 A, WRERTGRTFL***A***KNSSHTLLQ (The amino acid at the predicted methylation site in each peptide sequence is marked as bold and underlined, while the mutated site (K to A) is bold, italicized, and underlined).

Post-translational modification mass spectrometry

Methylation sites on recombinant hKDM5A 1-1090 before or after SMYD2 methylation were determined by LC-MS/MS analysis at the UT Southwestern Proteomics Core. For the SMYD2 methylated samples, recombinant hKDM5A was methylated as described in the in vitro methylation assay section including all control reactions, with the following modifications: ^{3}H-SAM was replaced with SAM (New England BioLabs, B9003S), and the reactions were scaled up 3 times to have sufficient starting material for LC-MS/MS analysis of post-translational modifications on hKDM5A 1-1090. Samples were digested with elastase or chymotrypsin prior to LC-MS/MS analysis on either an Orbitrap Fusion Lumos or QExactive HF mass spectrometer (Thermo), as previously described (54). Peptide quantification was done with CPFP (55). Methylation sites and methylation levels were determined by Mascot (at 1% FDR) and Proteome Discoverer (at 5% FDR) software by the UT Southwestern Proteomics Core staff. Data presented corresponds to reproducible results over at least two reactions and software programs.

ELISA-based demethylase assay

For the demethylase assay, recombinant hKDM5A (residues1-1090) was first methylated *in vitro* as described above, but after replacing ^{3}H-SAM with SAM (New England BioLabs, B9003S). Reactions were incubated at 30 °C for 1-1.5 h. 10 μl of this methylation reaction mixture was used as the KDM5A enzyme source for a 50 μl demethylation reaction using the Epigenase JARID Demethylase Activity/Inhibition Assay kit (Fluorometric assay, Epigentek, P-3083) with the following modifications applied to co-factor concentrations in the reaction mixture: 50 μM Fe^{2+}, 1 mM α-ketoglutarate and 2 mM ascorbate. The demethylation reaction was incubated at 37 °C for 45 min and processed per the manufacturer's instructions. KDM5A enzyme activity was measured by reading the fluorescence at 530 nm excitation and 590 nm emission using a microplate spectrophotometer (BMG Labtech).

Western blot-based demethylase assay

Recombinant hKDM5A (residues1-1090) was methylated *in vitro* as described above with SMYD2, but the reactions were incubated at 30 °C for 30 min. As a negative control reaction, SMYD2 was heat-inactivated at 65 °C for 25 min before adding to a control reaction mix. 15 μl of the methylation reaction mixture was used as the enzyme source for a 75 μl demethylation reaction using histone H3K4me3 (2.5 μg, Active Motif, 31210) as the substrate in reaction buffer (50 mM HEPES pH7.5, 2 mM ascorbate, 50 μM Fe^{2+},

and 1 mM α-ketoglutarate). Demethylation reactions were incubated at 37 °C for 2h and processed for Western blot analysis to detect H3K4me3 or H3K4me2 histone marks. Imaging and signal detection were performed using the Bio-Rad gel doc XR+ and signal quantification using ImageJ (https://imagej.net/).

RNA-seq

HCT116 KDM5A−/− cells transfected with *KDM5A* (WT or MUT) and GFP transfected HCT116 cells were sorted to enrich for GFP positive cells at the UT Southwestern Flow Cytometry Core. Total RNA from ~10^6 GFP positive cells was extracted using Trizol (Invitrogen, 15,596–026) and sent to Novogene for sequencing (30 M raw paired reads, NovaSeq PE150). Fastq files were aligned to the GRCh38 human reference genome using STAR v2.7.1a. The bam files were processed to remove duplicate reads using Picard MarkDuplicates from GATK v4.1.2. FPKM values for genes were obtained using Cufflinks v2.2.1 and TPM-normalized, then log-transformed. Genes with a value of $\log_2$FPKM = 0 in all samples were discarded from the analysis, and expression values linearized. Average (AVE) and standard deviation (STD) were calculated from replicates. Any gene with a relative standard deviation (100 × STD/AVE) greater than 70 was removed. Fold change values were calculated using linearized expression of HCT116 KDM5A−/− reconstituted with either WT or MUT KDM5A *versus* HCT116 KDM5A−/− transfected with empty vector (EV). Genes upregulated or downregulated by at least 1.5-fold were used for further analysis.

IP-mass spectrometry analysis

In vitro IP-MS analysis: To identify proteins that interact with methylated or un-methylated form of KDM5A, 10.8 mg of purified KDM5A protein (Flag-tagged, residue 1–1090 of KDM5A, commercially purchased from BPS Bioscience) was methylated using SMYD2 and SAM as described above in *in vitro* methyltransferase assay. Control methylation reactions were performed using heat inactivated SMYD2 (control 1) or with buffer (control 2). Total protein in native form was generated by lysing 2 × 10^7 HEK-293T cells in 2 ml of IP buffer (150 mM NaCl, 50 mM Tris-HCl pH 7.4, 0.5% IGEPAL CA-630) supplemented with protease inhibitors (Roche, 11836153001) and phosphatase inhibitors (Roche, 04906837001) on ice for 10 min. The lysates were cleared by centrifugation at 16,000*g* for 10 min at 4 °C. To the cleared HEK-293T cell lysates, either the total methylated KDM5A or the control reactions were added along with 200 µl of M2 beads (Sigma, A2220) and incubated at 4 °C overnight with rotation. Next day, M2 beads were collected by centrifugation (800*g* for 10 s) and washed five times with IP buffer. KDM5A was eluted from the beads by incubating them with 200 µl of 10 mg/ml Flag peptide (Sigma, F3290) for 2 h at 4 °C. Proteins in eluates were determined by LC-MS/MS analysis.

In vivo IP-MS analysis: To identify KDM5A interactors in cells, HEK-293T cells were transfected, as described above, with EV, WT KDM5A, MUT KDM5A or WT KDM5A plus SMYD2 expression constructs. After 24 h, transfected cells were processed for immunoprecipitation (IP). Briefly, cells were washed with 1XPBS at room temperature, put on ice, harvested by scrapping into cold 1XPBS, pelleted and lysed in two pellet volumes of IP buffer (50 mM Tris pH8.0, Sigma T-1503, 120 mM NaCl, RPI 523020–1000.0, and 0.5% Igepal CA-630, Sigma I3021–100 ml) supplemented with protease inhibitors (Roche, 11836153001) and phosphatase inhibitors (Roche, 04906837001). Cells were incubated on ice for 10 min and debris was separated by spinning at 3500 rpm in a microcentrifuge (Eppendorf 5424R) at 4 °C. The lysis step was repeated one more time and the supernatants were pooled for protein assay using BioRad DC kit (BioRad, 5000111). Protein lysates were pre-cleared with 80 µl of pre-equilibrated Protein G Plus Agarose Suspension (Millipore IP04–1.5 ml) in lysis buffer for 1.5 h on a rotator at 4 °C. For each IP, 12 mg of total protein was incubated with 80 µg of HA antibody (Abcam, 9110) overnight at 4 °C. Antibody–protein complexes were pulled down by incubating the IP reactions with 1.2 ml of pre-equilibrated Protein G Plus Agarose Suspension in lysis buffer at 4 °C for 1h and centrifugation at 840*g* for 20 s. Agarose beads were washed four times with lysis buffer and the immunoprecipitates were eluted by incubating with 0.1 M glycine (RPI, G36050–5000.0), pH 2.5, three times. Eluates from the first elution step was used for LC-MS/MS analysis.

Mass spectrometry analysis of protein-protein interactions: The quality of the IP eluates in both experiments were assessed using SDS-PAGE followed by silver staining. IP eluates containing approximately 1 to 2 µg of pulled down KDM5A were used for mass spectrometry analysis at the UT Southwestern Proteomics Core for LC–MS/MS based protein identification as described before (54). Briefly: Trypsin digests of lysate samples were run on a Thermo Orbitrap LC-MS/MS system and analyzed using Proteome Discoverer v.2.4 (Thermo) by searching against the human-reviewed protein database from UniProt. Raw data values obtained corresponded to the abundance of each detected peptide in the whole IP. Peptides with statistically significant values of detection were further analyzed. The abundance of each protein/peptide in each sample was normalized to the total abundance of the corresponding sample and KDM5A interactors were identified using a filtering criterion. To determine interactors of methylated *versus* un-methylated KDM5A using the *in vitro* IP-MS experiment, a protein was classified as a unique/preferred binding partner of methylated KDM5A if either the methylated/control one or the methylated/control two ratio was ≥ 2-fold and the other ratio was ≥ 1.5-fold. A protein was classified as a unique/preferred binding partner of un-methylated KDM5A if one ratio was ≤ 0.5-fold and the other ratio was ≤ 0.67-fold. To determine the interactors of MUT *versus* WT KDM5A in the presence of SMYD2 using *in vivo* IP-MS, we calculated the normalized peptide abundance from MUT or WT KDM5A in the presence of SMYD2 minus the normalized peptide abundance of EV and show

ASBMB

only values > 0. BioVenn was used to depict interactors unique or common to MUT or WT KDM5A in the presence of SMYD2 (https://www.biovenn.nl/index.php) (55).

Assessing KDM5A methylation in cells

HEK-293T cells were plated as described in the ***Transfections*** section and transfected with GFP (1.6 μg/150 mm dish) and EV or SMYD2 (15.2 μg/150 mm dish) plasmids. Twenty-four hours post transfection, cells were collected, washed and lysed in IP buffer as described in *In vivo IP-MS analysis*. Lysates were precleared with 50 μl pre-equilibrated Protein G Plus Agarose Suspension (Millipore IP04–1.5 ml) in lysis buffer for 1 h on a rotator at 4 °C. Endogenous KDM5A was immunoprecipiated from lysates (2 mg of total protein) of EV or SMYD2 over-expressing cells using 16 μg KDM5A antibody (Bethyl, A300–897A-M) overnight at 4 °C. The next day, IP complexes were pulled down with 180 μl of pre-equilibrated Protein G Plus Agarose Suspension at 4 °C for 1h and centrifugation at 840 *g* for 20 s. Agarose beads were washed with IP buffer four times and the immunoprecipitated products were eluted by incubating with 0.1 M glycine (RPI, G36050–5000.0). Endogenous KDM5A levels or KDM5A methylation status in eluates was assessed by probing with anti-KDM5A (Cell Signaling Technologies) or with anti-mono/di methyl lysine (PTM Bio, PTM-602) antibody by Western blot on the identical membrane (see Western blot analysis section). SMYD2 overexpression levels were measured in the input by Western blot using HSP90 as a loading control.

To compare the methylation status of full-length WT *versus* full-length K1063A MUT KDM5A in cells, HEK293T cells were transfected with GFP (1.6 μg/150 mm dish), HA-KDM5A (WT or MUT at 9.6 μg/150 mm dish) and SMYD2 (EV, WT or catalytic inactive Y240F (CI) at 15.2 μg/150 mm dish). Twenty-six hours post transfection, cells were collected, washed, lysed and precleared as described above. Ectopically expressed HA-tagged KDM5A from 1.4 mg of total protein was immunoprecipitated using anti-HA antibody (Abcam, ab9110, 8.4 μg) overnight at 4 °C. The next day, the complexes were pulled down using 168 μl of pre-equilibrated Protein G Plus Agarose suspension. The remaining steps of the immunoprecipitation and the detection of KDM5A methylation were performed as described above. Western blots were also run to measure starting input material (KDM5A detection with anti-HA antibody and SMYD2 detection with anti-SMYD2, using HSP90 and cyclophilin as loading controls).

Western blot analysis

Cells were lysed in RIPA buffer (50 mM Tris pH 7.4, 150 mM NaCl, 0.1% SDS, 1% IGEPAL CA-630, 0.5% sodium deoxycholate, 1 mM EDTA) supplemented with protease inhibitors (Roche, 11,836,153,001) for 30 min on ice with occasional vortexing. Cell debris was pelleted (19,000*g* for 10 min), protein concentration was quantified, and equal amounts of protein ran on a 4 to 15 or 4 to 20% SDS gradient gel (BioRad). Protein was transferred onto PVDF membranes (Thermo Scientific, 88518) and probed using indicated antibodies. Imaging and signal detection were performed on Li-Cor Odyssey Fc systems (LICORbio) and signals were quantified using Image Studio Lite. When necessary due to anti-body lack of compatibility (anti-mono/dimethyl pan antibody *versus* anti-HA or anti-KDM5A antibody probed on the same membrane), membranes was washed twice with stripping buffer (62.5 mM Tris pH 6.8, 2% SDS), and in the third buffer wash, stripping buffer was supplemented with 113.5 mM β-mercaptoethanol and incubated at 55 °C for 30 min. Then, the membranes were rocked at RT for another 30 min before extensive washing with water then with 1x TBST then probed with secondary antibody and developed to ensure the original signal from the anti-mono/dimethyl pan antibody was gone before re-probing with anti-KDM5A or anti-HA antibody.

Chromatin immunoprecipitation and sequencing (ChIP-seq)

HCT116 KDM5A−/− cells were transfected as described above with empty vector (EV), wild type (WT) or mutant (MUT) *KDM5A*. After 24 h of transfection, cells were processed for chromatin Immunoprecipitation (ChIP) with the Zymo-Spin ChIP kit (Zymo Research, D5210) following manufacturer instructions. Cells were crosslinked with 1% formaldehyde (Thermofisher, 28908) for 10 min at room temperature, then the reaction quenched by adding 125 mM glycine for 5 min. Crosslinked cells were washed thrice with cold 1X PBS and collected, then incubated in nuclei isolation buffer containing 1X protease inhibitors (Roche) for 5 min on ice. Isolated nuclei were spun down (300*g*, 2 min at 4 °C) and resuspended in chromatin lysis buffer containing 1X protease inhibitors. Chromatin shearing was performed with a Bioruptor (Diagenode) (30 s ON and 30 s OFF at highest power for 25 cycle at 4 °C). Sheared chromatin was clarified at 20,000 *g* for 15 min at 4 °C and the chromatin shearing efficiency verified by agarose gel electrophoresis with an observed DNA fragment length between ∼250 bp and ∼750 bp. 50 μg of chromatin from each sample was diluted 10-fold with ChIP dilution buffer (final volume of 1 ml) and incubated overnight with 1.5 μg of rabbit polyclonal anti-histone H3K4me3 antibody (Millipore, 07–473) or normal rabbit IgG (Santa Cruz, sc2027) as a control at 4 °C on a rotator. An input fraction corresponding to 10% of the chromatin used for immunoprecipitation was kept aside for normalization of ChIP enrichment. Protein-antibody complexes were captured using ZymoMag Protein A magnetic beads and washed sequentially with Chromatin Wash Buffers I, II, and III (once each) before being subjected to reverse crosslinking and DNA extraction as per the kit instructions. Quality of immunoprecipitated DNA was assessed on a Bioanalyzer (Agilent 2100, Agilent Technologies), and the concentration was determined using Qubit 2.0 Fluorometer (Invitrogen).

Sequencing libraries were prepared with 10 ng of immunoprecipitated DNA using the KAPA HTP Library Preparation Kit (Kapa Biosystems, KR0426). After end repair, 3′

A-tailing and ligation to barcoded multiplex adapters, the library was PCR amplified and purified with Ampure XP beads (Beckman Coulter, A63880). Library size and distribution were examined on an Agilent Bioanalyzer, quantified on a Qubit, normalized and run on the Illumina HiSeq 2500 sequencing system (Illumina) equipped with a mid-output flow cell at a read length of 2 x 100 bp. Sequencing reads were trimmed and mapped to the human reference genome (hg19) using Bowtie2 (v 2.5.4) (Langmead and Salzburg, 2012) and further analyzed by FastQ Screen (v 0.11.4). Uniquely mapped reads after duplicate removal resulted in 22,551,657 reads in EV, 20,362,784 reads in WT, 17,880,484 reads in MUT and 20,655,266 reads in combined IgG samples. Peak calling relative to genome background was performed using MACS2 (Model based analysis of ChIP-seq) set at default parameters (FDR cutoff is 0.05). Both narrow and broad peaks were called and annotated using the HOMER tool after normalization with respect to the corresponding input sample. A combined profile plot of all MACS peaks over a genomic region between 5 kb upstream and 5 kb downstream to the TSS (Transcription Start Site) was generated using the plotProfile tool (deepTools) (Diaz *et al.*, 2012). Normalized bigWig files were generated using deepTools (v 3.5.6, bamCompare) to visualize continuous-valued data tracks in IGV (Integrated Genomics Viewer, Robinson *et al.*, 2011). For calculation of tag density within defined genomic coordinates across samples, all peak regions were combined into a parent ".bed" file (RPM.combined.bed, normalized Reads per Million (RPM)) and annotated with HOMER. Resulting combined peaks and the corresponding tag density values across samples were compared using IGV and subjected to various filters in excel spreadsheets. Peaks demonstrating mutant specific decrease in H3K4me3 enrichment were identified by first setting filters for peaks with similar tag densities in EV and WT (EV/WT tag density ratio ≥ 0.9 & ≤ 1.1) followed by a second filter to select for peaks in MUT sample with a tag density fold difference of greater than or equal to 1.2 compared to WT (WT/MUT ≥ 1.2). Peaks demonstrating enhanced demethylation in the mutant (mutant enhanced) were defined as EV/WT tag density ratio ≥ 1.2 AND WT/MUT tag density ratio ≥ 1.2. Peaks resulting from these filters were subjected to further analysis.

Cell cycle analysis

HCT116 KDM5A−/− cells were transfected with either WT or MUT KDM5A in the presence of GFP as described in the ***Transfections*** section. At 48 and 72 h post transfection, approximately two million cells were collected, washed once with 1x PBS and fixed in ice cold 70% ethanol and incubated on ice for 30 min. Once the fixing step was completed, ethanol was removed, and cells were washed with 1x PBS twice by spinning at 850*g* for 5 min at 4 °C in each step. Cell pellets were resuspended in 500 µl of 1x PBS supplemented with 100 µg/ml RNaseA (Sigma, R5503) and 500 µl of 1x PBS supplemented with 50 µg/ml propidium iodide (Sigma, P4170–25 MG), and cell cycle distribution was analyzed by flow cytometry (FACS). Alternatively, at indicated time points after transfection, two million cells were collected by spinning at 300×*g* for 5 min at RT. Cell pellets were resuspended in 1 ml of phenol red free RPMI1640 (Gibco, 11,835–030) supplemented with 5% FBS (Gibco, 26,140–079) and 2 µg/ml Hoechst33342 (Tocris Bioscience 5117/50) and incubated at 37 °C for 10 min before cell cycle distribution was analyzed by Flow Cytometry. Percentage of cells in various cell cycle stages was determined using FlowJo software (https://www.flowjo.com/). All flow cytometry experiments, including data acquisition and analysis, were performed at the UT Southwestern Flow Cytometry Core.

Determination of KDM5A and SMYD2 co-target genes

The aggregate of KDM5A targets identified by ChIP-seq in HCT116 (39) and in MCF7 (GSE28337) cells were overlapped with SMYD2 targets determined by ChIP-seq in MDA-MB231 cells (56) using BioVenn (https://www.biovenn.nl/index.php). Corresponding data are shown in Figure S5*C* and Data Set S3.

Statistical analysis

Unless otherwise indicated in figure legends, p values comparing groups are from two-tailed t-tests with unequal variances, calculated in Excel. * = $p \leq 0.05$, ** = $p \leq 0.01$, *** = $p \leq 0.001$, ns = not significant.

KDM5A structure modeling and sequence alignments

The 3D structure for KDM5A protein was generated using AlphaFold software. Various domains identified by UniProt (P29375) were marked with different colors and key amino acid residues highlighted as noted in the figure legends. Further structural information was obtained from reference (57). Amino acid sequences for KDM5A and KDM5B were obtained from UniProt (P29375 and Q9UGL1) and sequence alignment was performed using CLUSTAL 2.1 multiple sequence alignment (https://www.ebi.ac.uk/jdispatcher/msa/clustalo).

Data availability

All RNA-seq data have been deposited under GEO Submission GSE297614. ChIP-seq data have been deposited under GEO Submission GSE297612. Mass spectrometry data has been deposited in MassIVE database under Submission MSV000100328.

Supporting information—This article contains supporting information.

Acknowledgments—Purified recombinant SMYD2, G9A and p53 were a generous gift from Dr Cheng-Ming Chiang, UT Southwestern Medical Center, Dallas, Texas. Purified histones were a gift from the laboratory of Dr Bing Li. The authors thank the UT Southwestern Proteomics Core facility and especially Joseph Otto for help in performing and analyzing proteomics experiments and acknowledge the efforts and helpful comments of former members of the Martinez laboratory.

Author contributions—T. A. T., G. G., C. N., and R. T. investigation; T. A. T., G. G., C. N., F. G., L. G. visualization; T. A. T., G. G., S. Y. W., and A. L. methodology; T. A. T., G. G., C. N., F. G., A. L., L. G., and E. D. M. formal analysis; T. A. T. validation; T. A. T., G. G., C. N., and E. D. M. writing–review and editing; G. G., C. N., F. G., and A. L. data curation; S. Y. W. resources; E. D. M. conceptualization; E. D. M. writing–original draft; E. D. M. funding acquisition; E. D. M. supervision.

Funding and additional information—This work was partly supported by The Welch Foundation (I-1878 to E. D. M.), the NIH 1R01CA251698-01 and 1R01CA288743-01A1 as well as the Chung-Ho Chen Cancer Research Fund to S. Y. W., and the NIH (Lung Cancer SPORE P50 CA070907 DRP and R03CA273480 to E. D. M. with a diversity supplement to C. N.).

Conflict of interest—The authors declare that they have no conflicts of interest with the content of this article. E. D. M. is the co-founder of Raphael Pharmaceuticals, LLC.

Abbreviations—The abbreviations used are: CA, catalytically active; ChIP, chromatin immunoprecipitation; CI, catalytically inactive; IP, immunoprecipitation.

References

1. Fan, T., Xie, J., Huang, G., Li, L., Zeng, X., and Tao, Q. (2024) PHF8/KDM7B: a versatile histone demethylase and epigenetic modifier in nervous system disease and cancers. *Epigenomes* **8**, 36
2. Gray, Z. H., Honer, M. A., Ghatalia, P., Yang, S., and Johnathan, R. W. (2025) 20 years of histone lysine demethylases: from discovery to the clinic and beyond. *Cell* **188**, 1747–1783
3. Manni, W., Jianxin, X., Weiqi, H., Chen, S., and Shi, H. (2022) JMJD family proteins in cancer and inflammation. *Signal. Transduct Target. Ther.* **7**, 304
4. Sarah, L., and Fujimori, D. G. (2023) Recent developments in catalysis and inhibition of the Jumonji histone demethylases. *Curr. Opin. Struct. Biol.* **83**, 102707
5. Song, Y. Q., Yang, G. J., Ma, D. L., Wanhe, W., and Chung-Hang, L. (2023) The role and prospect of lysine-specific demethylases in cancer chemoresistance. *Med. Res. Rev.* **43**, 1438–1469
6. Sterling, J., Menezes, S. V., Abbassi, R. H., and Munoz, L. (2021) Histone lysine demethylases and their functions in cancer. *Int. J. Cancer* **148**, 2375–2388
7. Sui, Y., Gu, R., and Janknecht, R. (2021) Crucial functions of the JMJD1/KDM3 epigenetic regulators in cancer. *Mol. Cancer Res.* **19**, 3–13
8. Wang, Z., and Liu, H. (2024) Roles of lysine methylation in glucose and lipid metabolism: functions, regulatory mechanisms, and therapeutic implications. *Biomolecules* **14**, 862
9. Vinogradova, M., Gehling, V. S., Gustafson, A., Shilpi, A., Charles, A. T., Catherine, W., *et al.* (2016) An inhibitor of KDM5 demethylases reduces survival of drug-tolerant cancer cells. *Nat. Chem. Biol.* **12**, 531–538
10. Zhang, Q. J., Chen, H. Z., Wang, L., Liu, D. P., Hill, J. A., and Liu, Z. P. (2011) The histone trimethyllysine demethylase JMJD2A promotes cardiac hypertrophy in response to hypertrophic stimuli in mice. *J. Clin. Invest.* **121**, 2447–2456
11. Zhang, Q. J., Tran, T. A. T., Wang, M., Ranek, M. J., Kokkonen-Simon, K. M., Gao, J., *et al.* (2018) Histone lysine dimethyl-demethylase KDM3A controls pathological cardiac hypertrophy and fibrosis. *Nat. Commun.* **9**, 5230
12. Hojfeldt, J. W., Agger, K., and Helin, K. (2013) Histone lysine demethylases as targets for anticancer therapy. *Nat. Rev. Drug Discov.* **12**, 917–930
13. Pedersen, M. T., and Helin, K. (2010) Histone demethylases in development and disease. *Trends Cell Biology* **20**, 662–671
14. Iwase, S., Lan, F., Bayliss, P., de la Torre-Ubieta, L., Huarte, M., Qi, H. H., *et al.* (2007) The X-linked mental retardation gene SMCX/JARID1C defines a family of histone H3 lysine 4 demethylases. *Cell* **128**, 1077–1088
15. Chen, Z., Zang, J., Whetstine, J., Hong, X., Davrazou, F., Kutateladze, T. G., *et al.* (2006) Structural insights into histone demethylation by JMJD2 family members. *Cell* **125**, 691–702
16. Rose, N. R., Ng, S. S., Mecinovic, J., Liénard, B. M., Bello, S. H., Sun, Z., *et al.* (2008) Inhibitor scaffolds for 2-oxoglutarate-dependent histone lysine demethylases. *J. Med. Chem.* **51**, 7053–7056
17. Schofield, C. J., and Zhang, Z. (1999) Structural and mechanistic studies on 2-oxoglutarate-dependent oxygenases and related enzymes. *Curr. Opin. Struct. Biol.* **9**, 722–731
18. Sanulli, S., Justin, N., Teissandier, A., Ancelin, K., Portoso, M., Caron, M., *et al.* (2015) Jarid2 methylation via the PRC2 complex regulates H3K27me3 deposition during cell differentiation. *Mol. Cell* **57**, 769–783
19. Gu, R., Kim, T. D., Song, H., Sui, Y., Shin, S., Oh, S., *et al.* (2023) SET7/9-mediated methylation affects oncogenic functions of histone demethylase JMJD2A. *JCI Insight* **8**, e164990
20. Sanchez, A., Buck-Koehntop, B. A., and Miller, K. M. (2022) Joining the PARty: PARP regulation of KDM5A during DNA repair (and transcription?). *Bioessays* **44**, e2200015
21. Krishnakumar, R., and Kraus, W. L. (2010) PARP-1 regulates chromatin structure and transcription through a KDM5B-dependent pathway. *Mol. Cell* **39**, 736–749
22. Kirtana, R., Manna, S., and Patra, S. K. (2020) Molecular mechanisms of KDM5A in cellular functions: facets during development and disease. *Exp. Cell Res.* **396**, 112314
23. Yang, G. J., Zhu, M. H., Lu, X. J., Liu, Y. J., Lu, J. F., Leung, C. H., *et al.* (2021) The emerging role of KDM5A in human cancer. *J. Hematol. Oncol.* **14**, 30
24. Hsu, C. L., Lo, Y. C., and Kao, C. F. (2021) H3K4 methylation in aging and metabolism. *Epigenomes* **5**, 14
25. Blair, L. P., Liu, Z., Labitigan, R. L., Wu, L., Zheng, D., Xia, Z., *et al.* (2016) KDM5 lysine demethylases are involved in maintenance of 3'UTR length. *Sci. Adv.* **2**, e1501662
26. Nishibuchi, G., Shibata, Y., Hayakawa, T., Hayakawa, N., Ohtani, Y., Sinmyozu, K., *et al.* (2014) Physical and functional interactions between the histone H3K4 demethylase KDM5A and the nucleosome remodeling and deacetylase (NuRD) complex. *J. Biol. Chem.* **289**, 28956–28970
27. Pavlenko, E., Ruengeler, T., Engel, P., and Poepsel, S. (2022) Functions and interactions of Mammalian KDM5 demethylases. *Front. Genet.* **13**, 906662
28. Petronikolou, N., Longbotham, J. E., and Fujimori, D. G. (2020) Extended recognition of the histone H3 tail by histone demethylase KDM5A. *Biochemistry* **59**, 647–651
29. Huang, J., Perez-Burgos, L., Placek, B. J., Sengupta, R., Richter, M., Dorsey, J. A., *et al.* (2006) Repression of p53 activity by Smyd2-mediated methylation. *Nature* **444**, 629–632
30. Saddic, L. A., West, L. E., Aslanian, A., Yates, J. R., 3rd, Rubin, S. M., Gozani, O., *et al.* (2010) Methylation of the retinoblastoma tumor suppressor by SMYD2. *J. Biol. Chem.* **285**, 37733–37740
31. Cho, H. S., Hayami, S., Toyokawa, G., Maejima, K., Yamane, Y., Suzuki, T., *et al.* (2012) RB1 methylation by SMYD2 enhances cell cycle progression through an increase of RB1 phosphorylation. *Neoplasia* **14**, 476–486
32. Zhang, X., Tanaka, K., Yan, J., Li, J., Peng, D., Jiang, Y., *et al.* (2013) Regulation of estrogen receptor alpha by histone methyltransferase SMYD2-mediated protein methylation. *Proc. Natl. Acad. Sci. U. S. A.* **110**, 17284–17289
33. Donlin, L. T., Andresen, C., Just, S., Rudensky, E., Pappas, C. T., Kruger, M., *et al.* (2012) Smyd2 controls cytoplasmic lysine methylation of Hsp90 and myofilament organization. *Genes Dev.* **26**, 114–119
34. Piao, L., Kang, D., Suzuki, T., Masuda, A., Dohmae, N., Nakamura, Y., *et al.* (2014) The histone methyltransferase SMYD2 methylates PARP1 and promotes poly(ADP-ribosyl)ation activity in cancer cells. *Neoplasia* **16**, 257–264

35. Hamamoto, R., Toyokawa, G., Nakakido, M., Ueda, K., and Nakamura, Y. (2014) SMYD2-dependent HSP90 methylation promotes cancer cell proliferation by regulating the chaperone complex formation. *Cancer Lett.* **351**, 126–133
36. Kirtana, R., Manna, S., and Patra, S. K. (2023) KDM5A noncanonically binds antagonists MLL1/2 to mediate gene regulation and promotes epithelial to mesenchymal transition. *Biochim. Biophys. Acta Gene Regul. Mech.* **1866**, 194986
37. Qu, Q., Takahashi, Y. H., Yang, Y., Hu, H., Zhang, Y., Brunzelle, J. S., *et al.* (2018) Structure and conformational dynamics of a COMPASS histone H3K4 methyltransferase complex. *Cell* **174**, 1117–1126.e12
38. Mishra, S., Van Rechem, C., Pal, S., Clarke, T. L., Chakraborty, D., Mahan, S. D., *et al.* (2018) Cross-talk between lysine-modifying enzymes controls site-specific DNA amplifications. *Cell* **175**, 1716
39. Hu, D., Jablonowski, C., Cheng, P. H., AlTahan, A., Li, C., Wang, Y., *et al.* (2018) KDM5A regulates a translational program that controls p53 protein expression. *iScience* **9**, 84–100
40. Deogharia, M., Venegas-Zamora, L., Agrawal, A., Shi, M., Jain, A. K., McHugh, K. J., *et al.* (2024) Histone demethylase KDM5 regulates cardiomyocyte maturation by promoting fatty acid oxidation, oxidative phosphorylation, and myofibrillar organization. *Cardiovasc. Res.* **120**, 630–643
41. Varaljai, R., Islam, A. B., Beshiri, M. L., Rehman, J., Lopez-Bigas, N., and Benevolenskayas, E. V. (2015) Increased mitochondrial function downstream from KDM5A histone demethylase rescues differentiation in pRB-deficient cells. *Genes Dev.* **29**, 1817–1834
42. Wang, L., Gao, Y., Zhang, G., Li, D., Wang, Z., Zhang, J., *et al.* (2020) Enhancing KDM5A and TLR activity improves the response to immune checkpoint blockade. *Sci. Transl. Med.* **12**, eaax2282
43. Kumbhar, R., Sanchez, A., Perren, J., Gong, F., Corujo, D., Medina, F., *et al.* (2021) Poly(ADP-ribose) binding and macroH2A mediate recruitment and functions of KDM5A at DNA lesions. *J. Cell Biol.* **220**, e202006149
44. Olsen, J. B., Cao, X. J., Han, B., Chen, L. H., Horvath, A., Richardson, T. I., *et al.* (2016) Quantitative profiling of the activity of protein lysine methyltransferase SMYD2 using SILAC-based proteomics. *Mol. Cell. Proteomics* **15**, 892–905
45. Tate, J. G., Bamford, S., Jubb, H. C., Dawson, E., Kok, C., Clements, J., *et al.* (2019) COSMIC: the catalogue of somatic mutations in cancer. *Nucleic Acids Res.* **47**, D941–D947
46. Marcon, E., Ni, Z., Pu, S., Turinsky, A. L., Trimble, S. S., Olsen, J. B., *et al.* (2014) Human-chromatin-related protein interactions identify a demethylase complex required for chromosome segregation. *Cell Rep.* **8**, 297–310
47. Yheskel, M., Sidoli, S., and Secombe, J. (2023) Proximity labeling reveals a new in vivo network of interactors for the histone demethylase KDM5. *Epigenetics Chromatin* **16**, 8
48. Gong, F., Clouaire, T., Aguirrebengoa, M., Legube, G., and Miller, K. M. (2017) Histone demethylase KDM5A regulates the ZMYND8-NuRD chromatin remodeler to promote DNA repair. *J. Cell Biol.* **216**, 1959–1974
49. Gonzalez-Mantilla, A. J., Moreno-De-Luca, A., Ledbetter, D. H., and Martin, C. L. (2016) A cross-disorder method to identify novel candidate genes for developmental brain disorders. *JAMA Psychiatry* **73**, 275–283
50. Abrahams, B. S., Arking, D. E., Campbell, D. B., Mefford, H. C., Morrow, E. M., Weiss, L. A., *et al.* (2013) SFARI gene 2.0: a community-driven knowledgebase for the autism spectrum disorders (ASDs). *Mol. Autism* **4**, 36
51. Abu-Farha, M., Lanouette, S., Elisma, F., Tremblay, V., Butson, J., Figeys, D., *et al.* (2011) Proteomic analyses of the SMYD family interactomes identify HSP90 as a novel target for SMYD2. *J. Mol. Cell Biol.* **3**, 301–308
52. Capes-Davis, A., Reid, Y. A., Kline, M. C., Storts, D. R., Strauss, E., Dirks, W. G., *et al.* (2013) Match criteria for human cell line authentication: where do we draw the line? *Int. J. Cancer* **132**, 2510–2519
53. Gazdar, A. F., Girard, L., Lockwood, W. W., Lam, W. L., and Minna, J. D. (2010) Lung cancer cell lines as tools for biomedical discovery and research. *J. Natl. Cancer Inst.* **102**, 1310–1321
54. Guo, X., Trudgian, D. C., Lemoff, A., Yadavalli, S., and Mirzaei, H. (2014) Confetti: a multiprotease map of the HeLa proteome for comprehensive proteomics. *Mol. Cell. Proteomics* **13**, 1573–1584
55. Hulsen, T., de Vlieg, J., and Alkema, W. (2008) BioVenn - a web application for the comparison and visualization of biological lists using area-proportional Venn diagrams. *BMC Genomics* **9**, 488
56. Zeng, Y., Qiu, R., Yang, Y., Gao, T., Zheng, Y., Huang, W., *et al.* (2019) Regulation of EZH2 by SMYD2-Mediated lysine methylation is implicated in tumorigenesis. *Cell Rep.* **29**, 1482–1498.e1484
57. Horton, J. R., Engstrom, A., Zoeller, E. L., Liu, X., Shanks, J. R., Zhang, X., *et al.* (2016) Characterization of a linked jumonji domain of the KDM5/JARID1 family of histone H3 lysine 4 demethylases. *J. Biol. Chem.* **291**, 2631–2646